The evolution of stellar triples:

The most common evolutionary pathways

S. Toonen[1,2,3], S. Portegies Zwart[3], A.S. Hamers[4,5], and D. Bandopadhyay[1]

[1] Institute of Gravitational Wave Astronomy, School of Physics and Astronomy, University of Birmingham, Birmingham, B15 2TT, United Kingdom
   e-mail: `toonen@star.sr.bham.ac.uk`
[2] Anton Pannekoek Institute for Astronomy, University of Amsterdam, 1090 GE Amsterdam, The Netherlands
[3] Leiden Observatory, Leiden University, PO Box 9513, NL-2300 RA Leiden, the Netherlands
[4] Institute for Advanced Study, School of Natural Sciences, Einstein Drive, Princeton, NJ 08540, USA
[5] Max-Planck Institute for Astrophysics, Karl-Schwarzschild-Str. 1, D-85741 Garching, Germany

ABSTRACT

Context. Many stars do not live alone, but instead have one or more stellar companions. Observations show that these binaries, triples and higher-order multiples are common. Whereas the evolution of single stars and binaries have been studied extensively, the same is not true for the evolution of stellar triples.
Aims. To fill this gap in our general understanding of stellar lives, we aim to systematically explore the long-term evolution of triples and to map out the most common evolutionary pathways that triples go through. We quantitatively study how triples evolve, which processes are most relevant, and how this differs from binary evolution.
Methods. We simulate the evolution of several large populations of triples with a population synthesis approach. We make use of the triple evolution code TRES to simulate the evolution of each triple in a consistent way; including three-body dynamics (based on the secular approach), stellar evolution and their mutual influences. We simulate the evolution of the system up until mass transfer starts, the system becomes dynamically unstable, or a Hubble time has passed.
Results. We find that stellar interactions are common in triples. Compared to a binary population, we find that the fraction of systems that can undergo mass transfer is $\sim 2-3$ times larger in triples. Moreover, whereas in binaries the orbits typically reach circularisation before Roche-lobe overflow, this is not true anymore in triples. In our simulations, about 40% of systems retain an eccentric orbit. Additionally, we discuss various channels of triple evolution in detail such as those where the secondary or the tertiary is the first star to initiate a mass transfer event.

Key words. stars: evolution, binaries: general, binaries: close

1. Introduction

Stellar systems are the building blocks of stellar clusters and galaxies. Some of them consist of a single star like our Solar system, but the majority of stars are members of binaries, triples, and higher order hierarchies. The fraction of triples is considerable. About 10% of systems with F- & G-type primary stars are triples. (Eggleton & Tokovinin 2008; Raghavan et al. 2010; Tokovinin 2014; Moe & Di Stefano 2017). The fraction gradually increases for higher mass primaries, reaching levels of several tenths of percents for early B-type and O-type stars (Remage Evans 2011; Sana et al. 2014; Moe & Di Stefano 2017). The overall multiplicity fraction (that is having two or more companions) indicates that the majority of systems with O-type primaries are triples and higher-order multiples (Moe & Di Stefano 2017).

The evolution of single stars and binaries have been studied extensively, but this is not the case for the evolution of stellar triples. The evolution of triples iss complicated as it is a combination of stellar evolution, stellar interactions and three-body dynamics (see Toonen et al. 2016, for a review). An example of the latter are Lidov-Kozai (LK) cycles (Lidov 1962; Kozai 1962) in which secular gravitational effects induce eccentricity oscillations in the inner binary system (see Naoz 2016, for a comprehensive review). However, realistic stellar triples are not purely gravitational systems, because stars are objects with finite sizes and lifetimes, and non-static natures (e.g. evolving masses and radii). Due to stellar evolution, a triple can move in or out of the regime where three-body dynamics modify the system (e.g. Fabrycky & Tremaine 2007; Perets & Kratter 2012; Shappee & Thompson 2013; Hamers et al. 2013; Michaely & Perets 2014; Antonini et al. 2017; Toonen et al. 2018a; Hamers & Thompson 2019a,b). Therefore, to study the evolution of stellar triples consistently, stellar evolution and a full treatment of dynamics need to be taken into account simultaneously. Here we present the systematic exploration of the evolution of stellar triples with low and intermediate mass stars. What are the common evolutionary channels that these triple systems evolve through? Which evolutionary pathways are open to triples that are not open to isolated binaries, and how common are these channels? We address these questions using a population synthesis approach with the triple evolution code TRES (Toonen et al. 2016). In Sect. 2 we outline our model assumptions for the initial populations of triples and their evolution. We discuss the five most common evolutionary channels and their demographics in Sect. 3, and their dependence on our model assumptions in Sect. 4. We summarise our findings in Sect. 5.

2. Method

To construct a map of the most common evolutionary pathways that triples evolve through, we simulate the evolution of representative populations of triple star-systems. We focus on isolated, hierarchical, coeval, initially dynamically stable systems. The simulation of an individual triple is ceased if a Hubble time has passed (here taken as 13.5Gyr), or if the system becomes dynamically unstable, or if mass transfer commences. In Sect. 2.1 we describe the primordial triple populations adopted in this study, and in Sect. 2.2 our computational method using the triple population synthesis code the code TRES.

2.1. Primordial population

When a triple is sufficiently hierarchical, it can be described by an inner binary whose centre of mass is orbited by a distant star i.e. the outer star. The masses of the stars in the inner orbit are m_1 (primary mass) and m_2 (secondary mass), where $m_1 \geqslant m_2$ initially. The mass of the outer star is m_3 (tertiary mass). We define the inner and outer mass ratios as $q_{in} \equiv m_2/m_1$ and $q_{out} \equiv m_3/(m_1 + m_2)$. We note that the evolution of a star is primarily determined by its mass, with secondary effects due to metallicity (here taken as solar) and rotation[1]. The inner and outer orbits are given by the semimajor axis (a_{in} and a_{out}), the eccentricities (e_{in} and e_{out}), and the arguments of pericenter (g_{in} and g_{out}). The relative orientation of the two orbits with respect to one another is measured by the mutual inclination i. The longitudes of ascending nodes describe the orientation on the sky, but do not affect the evolution of the system (e.g. Harrington 1968; Naoz et al. 2013). The stellar rotation is described through the angular velocity $\Omega_1, \Omega_2, \Omega_3$ for the primary, secondary and tertiary, respectively.

We initialise our simulations with a population of stellar triples on the zero-age main-sequence (ZAMS). We apply three different models, named OBin, T14 and E09. The model OBin is based on our understanding of observed populations of primordial binaries, whereas model T14 and model E09 are based on triples as proposed by Tokovinin (2014) and Eggleton (2009). The sample of Tokovinin (2014) consists of 4847 FG-dwarfs within 67 pc, and the one used in Eggleton (2009) is a magnitude-limited sample of 4558 stellar systems. The models are described in detail below and an overview is given in Tbl. 1.

For all models, primary masses are drawn from an initial mass function based on Kroupa et al. (1993) in the range of 1-7.5$M_\odot$. In this mass range single stars evolve to the remnant stage within a Hubble time and do not experience a supernova explosion. In all models and their normalisation we require the primary masses to be above 0.08$M_\odot$ and companion masses above 0.008$M_\odot$ to exclude sub-stellar components. To calculate event rates, we assume that 15% of stellar systems are triples, and 50% are binaries (Tokovinin 2014). Furthermore, for Galactic rates we assume a constant star formation history of 3 $M_\odot$ per year for 10 Gyrs.

The mass ratios of model OBin and Tok14 (upper panel of Fig. 1) are based on our understanding of the mass ratio distribution of ZAMS binaries. These binaries exhibit mass ratios that are unbiased with respect to the primary and secondary mass i.e. a flat mass ratio distribution between 0 and 1 (e.g. Raghavan
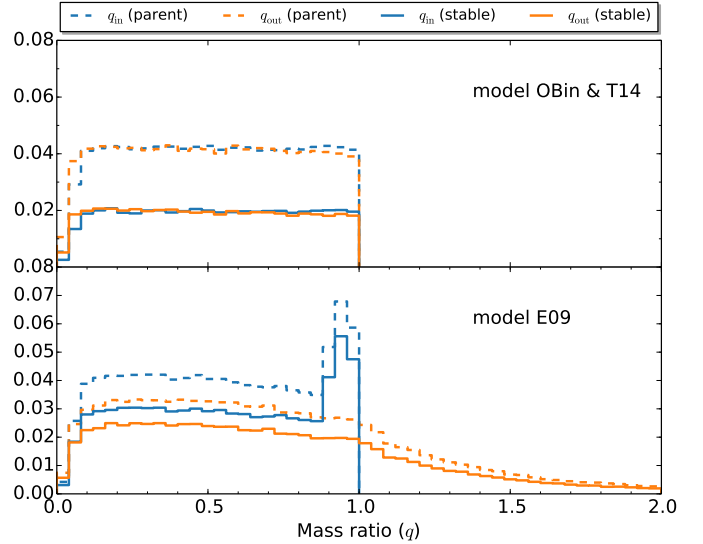
[1] Stellar rotation is known to affect the evolution of massive stars (e.g. Maeder & Meynet 2000), and in extreme cases it may lead to chemically homogeneous evolution. For the mass range studied in this paper, rotation is expected to be less important and therefore not taken into account here.


Fig. 1. Binned distributions of initial mass ratios for the inner and outer orbit (blue and orange lines). The dashed lines (normalised to unity) reflect the parent distributions from which we draw the mass ratios. The solid lines show the subset of systems that are dynamically stable according to the criterion by Mardling & Aarseth (1999) and that are used in the simulations. On the top, a flat mass ratio distribution is shown as used in model OBin and T14, whereas on the bottom the mass ratio distribution from model E09 is shown.

et al. 2010; Sana et al. 2012; Duchêne & Kraus 2013; Moe & Di Stefano 2017). Note that the mass ratio distributions decrease sharply at small mass ratios, as these systems would contain substellar companions. For model E09, the mass ratio distribution of the inner binaries (bottom panel of Fig. 1) is roughly flat except for an enhancement at nearly equal-mass stars. The mass ratio distribution of the outer binaries is also roughly flat for $0 < q \leqslant 1$, however, there is a tail that extends to high mass ratios. In model E09 the tertiary mass is not limited to the total mass of the inner binary. As a consequence, model E09 predicts ~ 10 times more systems with $m_3 > 7.5M_\odot$ compared to model OBin & Tok14 (which are not included in this study, see also Tbl. 2).

Next we describe the distributions of the inner and outer orbital separations (Fig. 3). For model OBin, we adopt a flat distribution in the logarithm of the orbital separation (e.g. Abt 1983; Kouwenhoven et al. 2007). The distribution of orbital separations ranges from $5R_\odot$ to $5 \cdot 10^6 R_\odot$. Even though the outer orbital separation is drawn from the same distribution as for the inner orbit, the distribution is biased to large orbital separations as we require $a_{out} > a_{in}$. The flat distribution is a classical assumption in binary population synthesis studies (e.g. Yungelson et al. 1993; de Kool & Ritter 1993; Portegies Zwart & Yungelson 1998; Nelemans et al. 2001; Hurley et al. 2002; Belczynski et al. 2002; Han et al. 2002; Izzard et al. 2009; Ruiter et al. 2009; Mennekens et al. 2010; Toonen et al. 2012; Claeys et al. 2014; van Haaften et al. 2013; Toonen et al. 2018b). It is a first-order approximation of the observed distribution of binary separations. However modifications have been proposed in which the shape of the distribution changes as a function of primary star mass (e.g. Duchêne & Kraus 2013; Moe & Di Stefano 2017). For example for Solar-type stars a log-normal distribution is preferred (e.g. Duquennoy & Mayor 1991; Raghavan et al. 2010), while
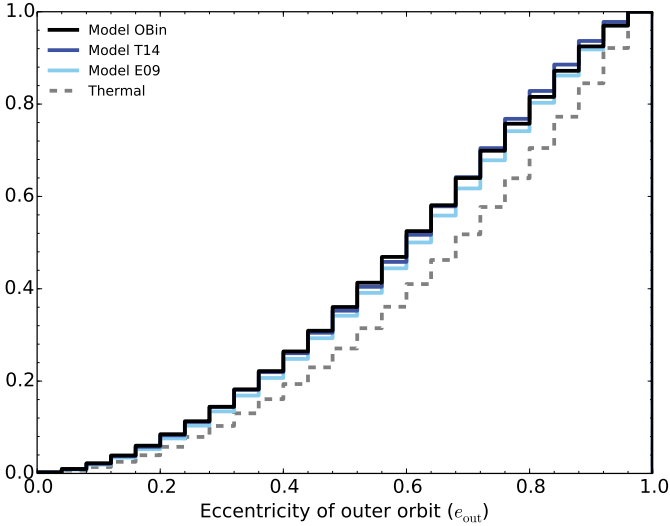
Fig. 2. Cumulative distribution of the initial eccentricity of the outer orbit normalised to unity. The dashed line shows the parent distribution (i.e. thermal distribution, Heggie 1975), and the solid lines represent the dynamically stable systems from each model used in our simulations.

a power-law with moderate slope is preferred for O- and B-type stars (Sana et al. 2012, 2014).

In the middle panel of Fig. 3, we show the orbital separations for model T14. In this model a log-normal distribution of periods (P in days) is assumed with mean $\mu = 5$ and dispersion $\sigma = 2.3$ (Duquennoy & Mayor 1991; Raghavan et al. 2010; Tokovinin 2014). Lastly, the primordial semimajor-axes of model E09 are shown in the bottom panel of Fig. 3. The inner orbital separations are similar to those of the log-normal distribution in model T14, but the outer orbits are generally wider by a factor of a few.

After drawing the inner and outer orbital separation according to the distributions described above (hereafter parent distributions), we require that the triple is dynamically stable. We use the stability criterion as given by Mardling & Aarseth (1999), see also Eq. 1. The resulting distributions of stable systems are shown as solid lines in Fig. 1 and Fig. 3. Comparing the populations before and after the stability cut shows that there are no signs of a strong bias with inner or outer mass ratio, however, the resulting distributions are biased to larger ratios of outer to inner semimajor axis. As a result, the inner orbit is biased towards shorter periods, and the outer orbit towards longer periods. We neglect the (dynamical and stellar) evolution on the pre-MS, and assume that on the zero-age MS the initial conditions are as described above (but see e.g. Moe & Kratter 2018).

For all models, we assume a thermal distribution of eccentricities (Heggie 1975) between 0 and 1. After removing the dynamically unstable systems the distribution of outer eccentricities is significantly affected (Fig. 2). The fraction of highly eccentric outer orbits is reduced, and overall the distribution has flattened. This is in line with the observed eccentricity distribution of wide binaries with projected separations larger than 50 au (Tokovinin & Kiyaeva 2016) based on the same 67pc sample as model T14. Generally observations show that the eccentricity distributions are less steep than the thermal distribution (Raghavan et al. 2010; Tokovinin & Kiyaeva 2016; Moe & Di Stefano 2017).

For the arguments of pericenter we adopt a uniform distribution between $-\pi$ and π, and for the inclination a uniform distribu-
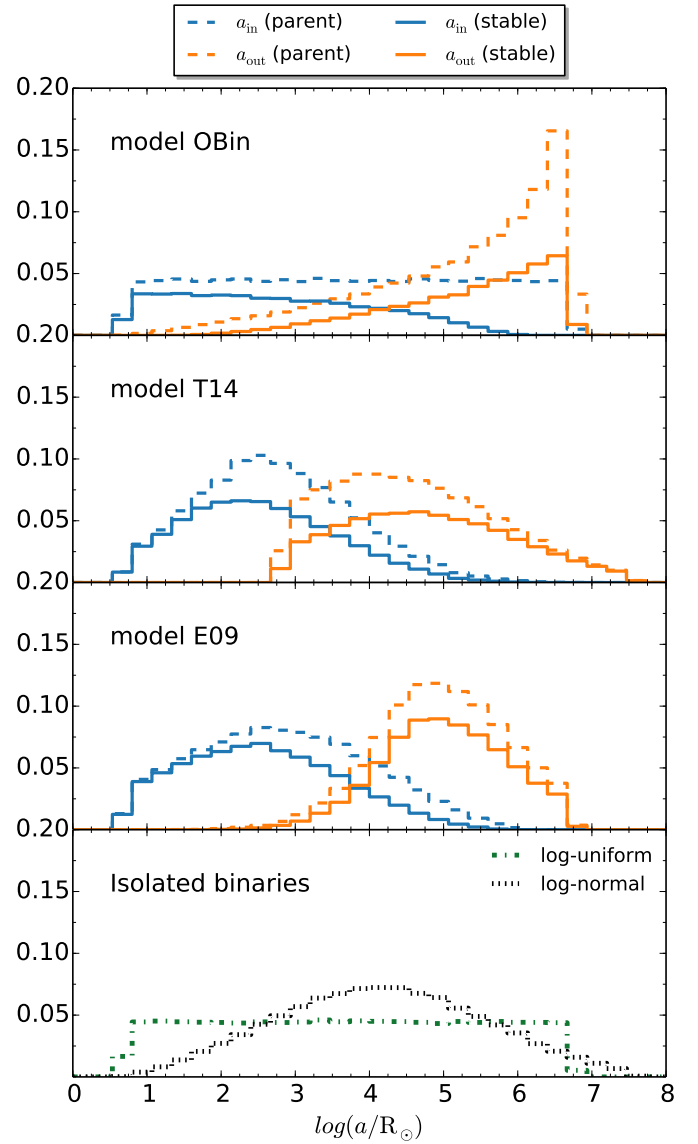

Fig. 3. Binned distributions of the initial inner and outer semimajor axis (blue and orange lines). The dashed lines (normalised to unity) reflect the parent distributions from which we draw the semimajor axes. The solid lines shows the subset of systems that are dynamically stable and that are used in the simulations. From top to bottom model OBin, T14 and E09 are shown. The bottom panel shows the distribution of semimajor axes that are commonly used for isolated binaries.

tion in the cosine of the inclination between 0 and π. Tokovinin (2017) finds that this is a good approximation for outer projected separations $\gtrsim 10^5 R_\odot$, but at $\lesssim 10^4 R_\odot$ there is more alignment (see also Fig. 3). The orbit alignment is stronger for systems with low-mass primaries ($m_1 < 1.2 M_\odot$, where the median initial primary mass in our simulation is $1.65 M_\odot$.) For the angular velocities of the initial stellar rotation, we follow Hurley et al. (2000).

2.2. TRES: modelling of triple evolution

In Toonen et al. (2016), we presented a code to simulate the evolution of hierarchical triple star systems; stellar evolution is combined with three-body dynamics. Single stellar evolution is

Table 1. Distributions of the initial binary parameter mass, mass ratio, orbital separation and eccentricity.

Parameter	Model OBin	Model T14	Model E09
Mass of binary primaries	Kroupa IMF [1]	Kroupa IMF [1]	Kroupa IMF [1]
Mass ratio	Uniform	Uniform	Model E09 [2]
Orbital separation	Uniform in log(a) [3]	Log-normal [4,5,6]	Model E09 [2]
Eccentricity	Thermal distribution [7]	Thermal distribution [7]	Thermal distribution [7]
Inclination	Uniform in cos(i)	Uniform in cos(i)	Uniform in cos(i)
Argument of pericenter	Uniform	Uniform	Uniform

Notes. [1] Kroupa et al. (1993); [2]Eggleton (2009); [3]Abt (1983); [4]Duquennoy & Mayor (1991); [5]Raghavan et al. (2010); [6]Tokovinin (2014); [7] Heggie (1975)

included through the fast stellar evolution code SeBa (Portegies Zwart & Verbunt 1996; Toonen et al. 2012). The code uses analytical formulae based on detailed single star tracks from Hurley et al. (2000) and provides parameters such that stellar radius and wind mass loss rates as a function of time. The orbits are solved using the secular approach (Harrington 1968; Ford et al. 2000; Naoz et al. 2013). The method is based on Hamers et al. (2013) and solves a set of first-order ordinary differential equations including secular three-body dynamics (accurate up to and including the octupole order), tides, general relativistic effects (Peters 1964), mass loss and mass transfer. Furthermore, precession from general relativistic effect (Blaes et al. 2002), due to tides acting on the stars (Smeyers & Willems 2001), and due to stellar rotation (Fabrycky & Tremaine 2007) are included. General tidal damping is included for stars with convective envelopes through equilibrium tides, with radiative envelopes through dynamical tides, and degenerate stars separately following Hurley et al. (2002). We adopt the Roche lobe equivalent for an eccentric orbit as derived by Sepinsky et al. (2007a) which is a function of eccentricity as well as the rotation of the stars. We assume that stellar winds are emitted spherically symmetrically and fast compared to the orbit, such that the effect on the orbit is adiabatic, and the orbit widens as $\dot{a}/a = -\dot{M}_{\text{total}}/M_{\text{total}}$ (e.g. Huang 1956, 1963). Furthermore, we assume the wind matter is not accreted by the stellar companions.

TRES is written within the Astrophysics Multipurpose Software Environment, or AMUSE (Portegies Zwart et al. 2009, 2013; Portegies Zwart & McMillan 2018). This is a component library with a homogeneous interface structure and can be downloaded for free at amusecode.org. In the AMUSE framework new and existing code from different domains can be easily coupled (e.g. stellar dynamics, stellar evolution, hydrodynamics and radiative transfer). As a result, the triple code can be easily extended in the future to include a detailed stellar evolution code or a direct N-body code to solve the dynamics of unstable triples.

For a full description of the TRES and an overview of relevant processes in triple evolution, see Toonen et al. (2016). In the following we highlight a number of processes.

– **Dynamical stability:** In this paper we focus on dynamically stable systems. Dynamically unstable systems tend to be short-lived and typically lead to dissociation or ionisation of the systems (e.g. van den Berk et al. 2007). Here we apply the stability criterion of Mardling & Aarseth (1999, 2001):

$$\frac{a_{\text{out}}}{a_{\text{in}}}\Big|_{\text{crit}} = \frac{2.8}{1-e_{\text{out}}}\left(1-\frac{0.3i}{\pi}\right)\cdot\left(\frac{(1+q_{\text{out}})\cdot(1+e_{\text{out}})}{\sqrt{1-e_{\text{out}}}}\right)^{2/5}. \quad (1)$$

Triples are unstable if $\frac{a_{\text{out}}}{a_{\text{in}}} < \frac{a_{\text{out}}}{a_{\text{in}}}|_{\text{crit}}$.

– **Lidov-Kozai cycles:** The lowest-order manifestation of three-body dynamics are the LK cycles (i.e. quadrupole order, Lidov 1962; Kozai 1962; Naoz 2016). Oscillations are induced in inclination and eccentricity of the inner binary system with a timescale of approximately (Kinoshita & Nakai 1999; Antognini 2015):

$$t_{\text{kozai}} = \alpha \frac{P_{\text{out}}^2}{P_{\text{in}}} \frac{m_1 + m_2 + m_3}{m_3} \left(1 - e_{\text{out}}^2\right)^{3/2}, \quad (2)$$

where P_{in} and P_{out} are the periods of the inner and outer orbit, respectively. α is a dimensionless quantity of order unity that depends weakly on the mutual inclination, inner eccentricity and argument of periastron. Within the test-particle approximation and circular initial orbits, the maximum eccentricity e_{max} is a function of the initial mutual inclination i_i as (Innanen et al. 1997):

$$e_{\text{max}} = \sqrt{1 - \frac{5}{3}\cos^2(i_i)}, \quad (3)$$

In this approximation the LK cycles only take place when the initial inclination is between 39.2-140.8°. When dropping some of the simplifications of this approximation (for example with non-zero initial eccentricities, realistic stellar masses ratios), the range of initial inclinations expands, higher-order levels of three-body dynamics can become important, and richer dynamical behaviour is expected.

– **Eccentric Lidov-Kozai regime:** The next order of approximation in the secular approach, the so-called octupole level, gives rise to more extreme dynamical interaction. In the octupole level, the system can experience a flip in its inclination (that is transition from prograde to retrograde or vice versa) or modulations in the eccentricity of the inner orbit that can reach close to unity (e.g. Ford et al. 2000; Blaes et al. 2002; Lithwick & Naoz 2011; Naoz et al. 2013; Shappee & Thompson 2013; Teyssandier et al. 2013). See also Naoz (2016) for an extensive review of the eccentric LK regime. Generally the octupole term is of importance if the octupole parameter $|\epsilon_{\text{oct}}| \gtrsim 0.001 - 0.01$ (Lithwick & Naoz 2011; Katz et al. 2011; Teyssandier et al. 2013; Li et al. 2014), where

$$\epsilon_{\text{oct}} = \frac{m_1 - m_2}{m_1 + m_2} \frac{a_{\text{in}}}{a_{\text{out}}} \frac{e_{\text{out}}}{1 - e_{\text{out}}^2}. \quad (4)$$

– **Semisecular evolution:** In the semisecular regime (e.g. Antonini & Perets 2012; Katz & Dong 2012; Luo et al. 2016) the triple is technically dynamically stable, but the hierarchy is moderate; the perturbations from the outer star on the inner orbit occur on a timescale that is comparable to or shorter than the dynamical times of the inner or outer binary. The
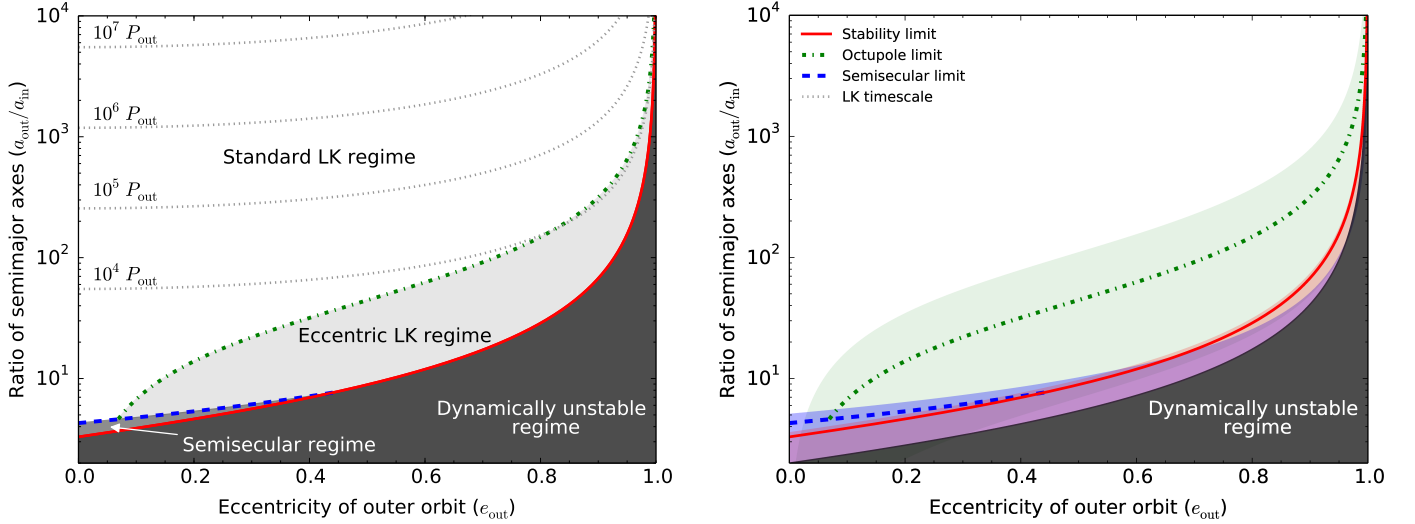
Fig. 4. Visualisation of the parameter space of the different dynamical regimes for triple systems (Sect. 2.2). On the left a triple with $m_1 = 1M_\odot$, $m_2 = 0.5M_\odot$, $m_3 = 0.75M_\odot$, and $i = 0°$ is assumed. The black dotted lines represent constant Lidov-Kozai timescales of value $10^4 P_{\rm out}$, $10^5 P_{\rm out}$, $10^6 P_{\rm out}$, and $10^7 P_{\rm out}$. The higher-order (octupole) term of the three-body interaction is important below the green dash-dotted line assuming a limit at $\epsilon_{\rm oct} = 0.005$. The triple is in the semisecular regime below the blue dashed line - assuming the inner eccentricity is 0.99 or can be reached during the LK cycles. For lower values of $e_{\rm in}$ the line moves downwards. The system is not dynamically stable below the red solid line. Below the blue dashed and red solid line the secular approach breaks down. On the right, the shaded areas represent how the boundary of the corresponding colour moves for different stellar masses, assuming m_2, m_3 in $[0.1, 0.9]M_\odot$. For the red shaded area we also take into account how the boundary of dynamical stability shifts when the inclination varies between $0 - 180°$.

regime is linked to rapid oscillations in the inner eccentricity and stellar collisions (e.g. Katz & Dong 2012; Seto 2013; Antonini et al. 2014; Antognini et al. 2014; Bode & Wegg 2014). The orbit-average treatment breaks down when:

$$\sqrt{1 - e_{\rm in}} \lesssim 5\pi q_{\rm out} \left(\frac{a_{\rm in}}{a_{\rm out}(1 - e_{\rm out})} \right)^3, \qquad (5)$$

as derived by Antonini et al. (2014) assuming the instantaneous quadrupole order torque, maximal torque at the periapsis approach and $e_{\rm in} \rightarrow 1$. The current study is based on the secular approach and does not consider the semisecular regime[2]. For the subset of moderate hierarchical systems, the maximum inner eccentricity is even higher than expected from secular theory, and likely leads to an earlier start of RLOF.

2.3. Visualisation of the dynamical regimes

The four processes described above give rise to different dynamical regimes in which each of them dominate over the other processes. Fig. 4 aims to discerns the parameter space of the dynamical regimes; for a single triple in Fig. 4a, whereas Fig. 4b aims to show how the boundaries between the regimes vary for triples with different mass ratios. In general, systems with $a_{\rm out}(1 - e_{\rm out})/a_{\rm in}$ smaller than a factor of a few are dynamically unstable. If the ratio is slightly larger the system is in the eccentric LK regime. If however, the inner eccentricity is (can become) large, and consequently the outer eccentricity is small, the system is in the semi-secular regime. For even larger ratios, the

---

[2] But see for example Toonen et al. (2017) for a study of wide triples that evolve into the semisecular regime due to stellar evolution, and lead to stellar collisions and transients on timescales of Gyrs.

systems experience standard LK cycles, with ever-larger periods up to and beyond a Hubble time.

To give a few examples, we have overplotted a number of known triples in Fig. 5. The nearest neighbour to the Sun is the stellar triple consisting of the Alpha Centauri system and Proxima Centauri. Within the uncertainties in $e_{\rm out} = 0.50^{0.08}_{0.09}$ (Kervella et al. 2017), the system is far away from the eccentric LK regime, the semisecular regime, and the dynamically unstable regime. Even if the inclination is favourable for LK cycles, the timescale is orders of magnitude larger than the outer period of approx 0.55Gyr.

Algol is a post-mass transfer system with an inclination around 95° (Kiseleva et al. 1998; Borkovits et al. 2010). The system is in the standard LK regime, but close to the eccentric LK-regime. The boundary of the eccentric LK-regime depends on the masses of the triple, as indicated by the green shaded area (Eq. 4). Specifically $a_{\rm out}/a_{\rm in}|_{\rm crit} \propto Q \equiv (m_1 - m_2)/(m_1 + m_2)$. The boundary of the eccentric LK-regime for Algol lies between the green dash-dotted line and the upper boundary of the green area, with $Q \sim 0.64$, $Q = \frac{1}{3}$, and $Q = 0.8$ respectively (Zavala et al. 2010, 2017). And so, the octupole term is likely not a dominant factor in the evolution of Algol. As the inclination is high, LK-cycles are expected (see also Kiseleva et al. 1998; Borkovits et al. 2004, 2010).

HIP101955 is a triple with well-determined orbital parameters (see e.g. Tokovinin & Latham 2017) in the green shaded area in Fig. 5. However, given its masses $m_1 = 0.74M_\odot$, $m_2 = 0.62M_\odot$, $Q \approx 0.09$ (Tokovinin & Latham 2017), the boundary of the eccentric LK-regime lies below the green dashed line ($Q = \frac{1}{3}$) by a factor $\frac{1}{3}/0.009 \approx 3.7$, such that HIP101955 is close to the eccentric LK regime, but likely not strongly affected by the octupole term. The same holds for the semi-secular regime. Strong LK cycles are expected with short timescales (≈ 560
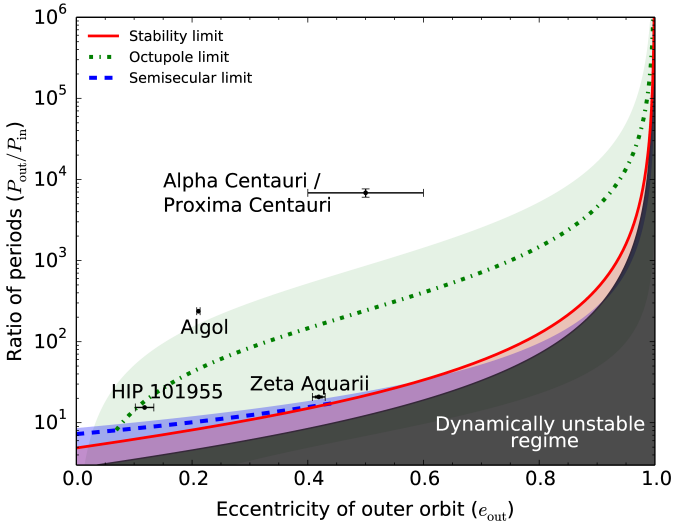
Fig. 5. Visualisation of the parameter space of the different dynamical regimes with several known triples. Systems that experience mass transfer are shown in the top panel. The bottom panel contains systems from the last two evolutionary channels. The figure is similar to Fig. 4b but with P_{out}/P_{in} on the y-axis instead of a_{out}/a_{in} because these are better measured in the current sample of overplotted observed triples overplotted. Depending on the method with which the orbit is studied, either the period or the semi-major axis may be determined more accurately.

years) that might be observable (Malogolovets et al. 2007; Xu et al. 2015).

Finally Zeta Aquarii is an interesting system as it lies close to the limit of dynamical stability. Given its high inner mass ratio ($m_1, m_2 \approx 1.4 M_\odot$) the octupole parameter is small (Tokovinin 2016), such that the octupole term is likely not very important. Regarding the semi-secular regime, as the outer mass ratio is small $q_{out} \approx 0.6/2.8$ compared to that of the blue dashed line $q_{out} = 1/2$, the boundary of the semi-secular regime of Zeta Aquarii is below the blue dashed line, bringing Zeta Aquarii further away from the semi-secular regime. Our adopted stability limit is not very sensitive to the outer mass ratio, but it is affected by the inclination of the system. As Zeta Aquarii has a retrograde orbit with an inclination of $140° \pm 10°$ (Tokovinin 2016) it is relatively more stable than a prograde equivalent system. The stability limit of Zeta Aquarii lies below the solid red line in Fig. 5. Ultimately, the proximity of Zeta Aquarii makes it an interesting system in the analysis of stability limits and strong three-body effects. With an age of about 3Gyr and LK cycles with timescales of about 48000 yr, the system has likely gone through many LK oscillations as corroborated by the inclination and the high inner eccentricity of 0.87 (Tokovinin 2016).

In the future when new triple systems are discovered, Figs. 4 and 5 can be used to assess which processes are relevant for that given triple. An interactive version of Fig. 4a is available at https://bndr.it/wr64f. The graphical interface allows the user to adjust the figure to any given triple.

3. Triple evolutionary pathways

Based on the models described in Sect. 2.1, the expected birthrate of all triples is about 150-175 systems per $1000 M_\odot$ of created stars (Tbl. 2). In the Milky Way, this translates to a birthrate of about one system every two years. As expected from the IMF, the majority of triples have low-mass stellar companions that do not leave the MS in a Hubble time. About 10% of triples have an intermediate mass primary (i.e. the initially most massive star in the inner binary), and ~1-2% has a high-mass primary which are the typical neutron star and black hole progenitors. In this study we focus on triple systems with intermediate mass primaries. The evolution of these triple star systems can be split up into five distinct evolutionary pathways:

- The primary star initiates mass transfer;
- The secondary star initiates mass transfer ;
- The tertiary star initiates mass transfer;
- The triple becomes dynamically unstable;
- The stars do not interact and the system remains intact for a Hubble time.

Fig. 6 shows the average frequency of each channel based on our triple population synthesis simulations. For 70-80% of triples, the stars will interact with each other at some point during their evolution. The most common outcome of triple evolution is mass transfer in the inner binary initiated by the primary. A few percent of triples destabilise or experience a mass transfer phase initiated by the secondary or tertiary, which all three is not expected to occur in isolated binaries without tertiary companions.

The birthrates of the five channels do not depend strongly on our assumptions for the primordial populations of triples (Tbl. 2). The rates vary within a factor of about two between the different models. In the subsequent sections, we discuss in more detail the characteristics of each channel.

3.1. Mass transfer initiated by the primary star

The most likely outcome for a triple with a $1 - 7.5 M_\odot$ mass primary is for the primary to fill its Roche lobe equivalent. This happens in 64-73% of all triples depending on the modelling of the primordial population.

Whereas isolated binaries are typically expected to circularise before (and remain circular during) the mass transfer phase [3], this is not the case for triple stars. An appreciable fraction of the inner orbits of triples is still eccentric at the onset of mass transfer (Fig. 8). The distribution of eccentricities of the inner orbits is bimodal; orbits are either circularised or highly eccentric. In the latter case, the median eccentricity is 0.86-0.89. Of the inner orbits 59-63% have circularised and 37-41% is eccentric (Fig. 10).

Whether or not an orbit circularises before the onset of mass transfer is a trade-off between tides and the LK cycles. The LK cycles can increase and decrease the eccentricity on a timescale that is strongly dependent on the periods of the inner and outer orbit (Eq. 2). In the absence of LK cycles, such as for isolated binaries, tides act to circularise the orbit. The characteristic timescale for orbital change due to tides is strongly dependent on the type of star and the ratio of the stellar radius to its orbital separation (Hut 1980). The interaction with tides and LK cycles, is one example of the interplay between stellar evolution and three-body dynamics in the evolution of stellar triples. The eccentricity distribution upon mass transfer demonstrates that three-body dynamics affects the evolution of a significant fraction of all triples.

---

[3] An exception occurs in massive binaries. Eldridge (2009) show that not all binaries with massive donor stars (and radiative envelopes) circularise during Case-B mass transfer events if the mass transfer occurs on a timescale that is shorter than what is required to circularise the orbit by tides.
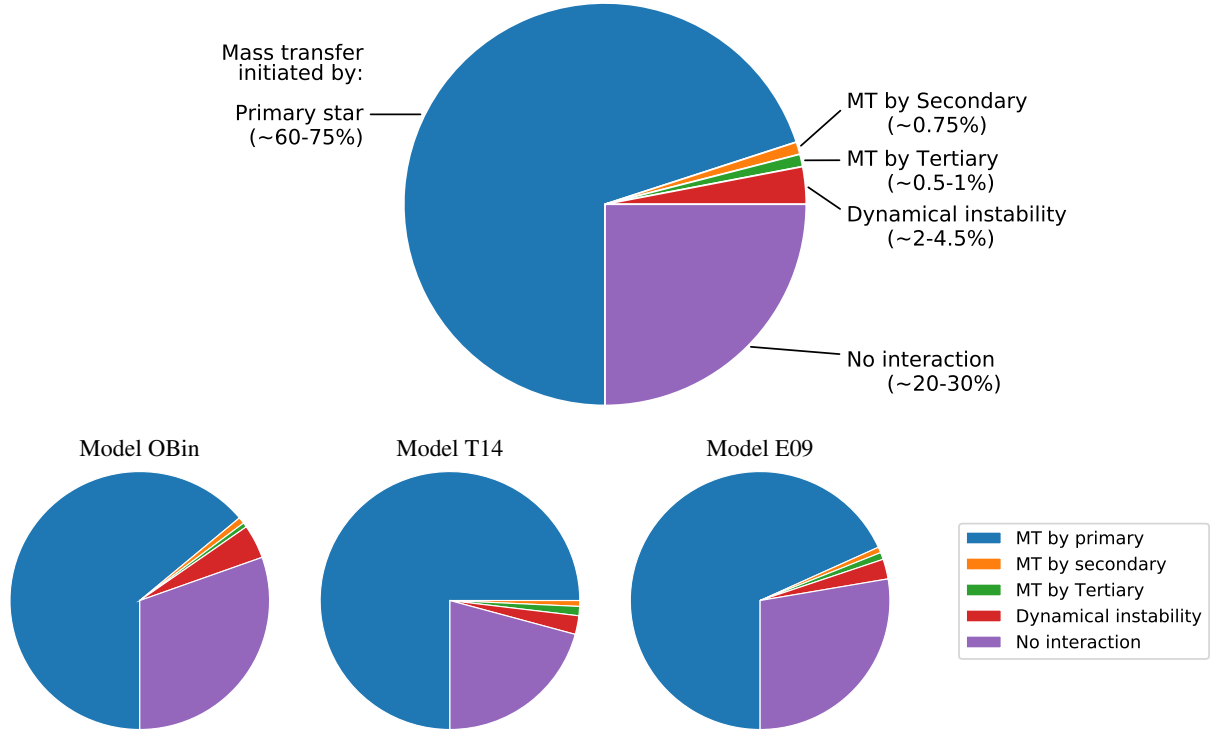
Fig. 6. Frequencies of the most abundant evolutionary channels for triples with intermediate-mass primaries based on a population synthesis simulation of triple systems using TRES. Mass transfer is common to occur in the evolution of a triple, and primarily with the primary star of the inner binary donating mass. On the top a summary of all models are shown indicating the range in expected frequencies. On the bottom row pie charts are shown for the different models individually.

Table 2. Birthrates of stellar triples per solar mass of stars (middle column) and in the Milky Way (right column). The bottom panel shows the occurrence rates of the most common evolutionary pathways of intermediate mass triples (that is initially $1 < m_1 \leq 7.5 M_\odot$ and $m_2, m_3 < 7.5 M_\odot$) based on a population synthesis simulation including a realistic mix of single, binary and triple stars (see Sect. 2).

| | | Total rate (per $10^4 M_\odot$) | | | Galactic rate (10^{-3} yr^{-1}) | | |
		OBin	T14	E09	OBin	T14	E09
Total birthrate		1740	1725	1489	522	517	45
- with low-mass ($m_1 \leq 1 M_\odot$)		1563	1544	1294	469	463	388
- with intermediate-mass ($1 < m_1 \leq 7.5 M_\odot$)		167	168	168	50	51	51
- with intermediate-mass ($1 < m_1 \leq 7.5 M_\odot, m_2, m_3 < 7.5 M_\odot$)		165	166	154	50	50	46
- with high-mass ($m_1 > 7.5 M_\odot$)		13	13	27	3.8	3.8	8.2
Birthrate per evolutionary channel							
Mass transfer initiated by:	primary star	105	125	106	30	35	30
	secondary star	1.3	1.2	1.1	0.3	0.3	0.3
	tertiary star	0.9	1.9	1.4	0.3	0.6	0.4
Dynamical instability		6.9	3.8	3.8	2.0	1.1	1.1
No interaction		40	34	42	17	13	15

An example of such an evolution is given by the following system: $m_1 = 1.63 M_\odot$, $m_2 = 0.82 M_\odot$, $m_3 = 2.06 M_\odot$, $i = 71.5°$, $a_{in} = 8.91 R_\odot$, $e_{in} = 0.57$, $g_{in} = -2.53$rad, $a_{out} = 750 R_\odot$, $e_{out} = 0.46$, $g_{out} = 1.55$rad on the ZAMS. Initially the system is detached, dynamically stable, and in the octupole regime with $\epsilon_{oct} = 0.0023$, see also Figs. 7. Correspondingly the timescale of the Lidov-Kozai cycles is short i.e. about 2680 years. After about 50 Myrs, when the inner eccentricity has increased to 0.61 and the Roche lobe of the primary has shrunken accordingly, the primary star fills its Roche lobe and initiates the mass transfer phase in a significantly eccentric orbit. Similar to this example, it is common for all systems of this evolutionary channel to be in the octupole regime, as can be seen by comparing Fig. 7

and Fig. 4. In model OBin and model E09 it entails about 45% (14%) of systems that have $\epsilon_{oct} > 0.001$ (0.01). The fraction increase to 61% (21%) respectively for model T14, as the inner and outer orbits tend to be closer together in this model. Fig. 7 also shows that the systems of this evolutionary channel are not only in the octupole regime at birth, but cover a range of dynamical regimes, which indicates a variable importance of the tertiary star and three-body dynamics.

The eccentricity is relevant for the subsequent evolution of the system; the mass transfer phase progresses differently when the orbit is eccentric instead of circularised due to the phase-dependency of the mass transfer when the orbit is eccentric (Layton et al. 1998; Regös et al. 2005; Lajoie & Sills 2011; van
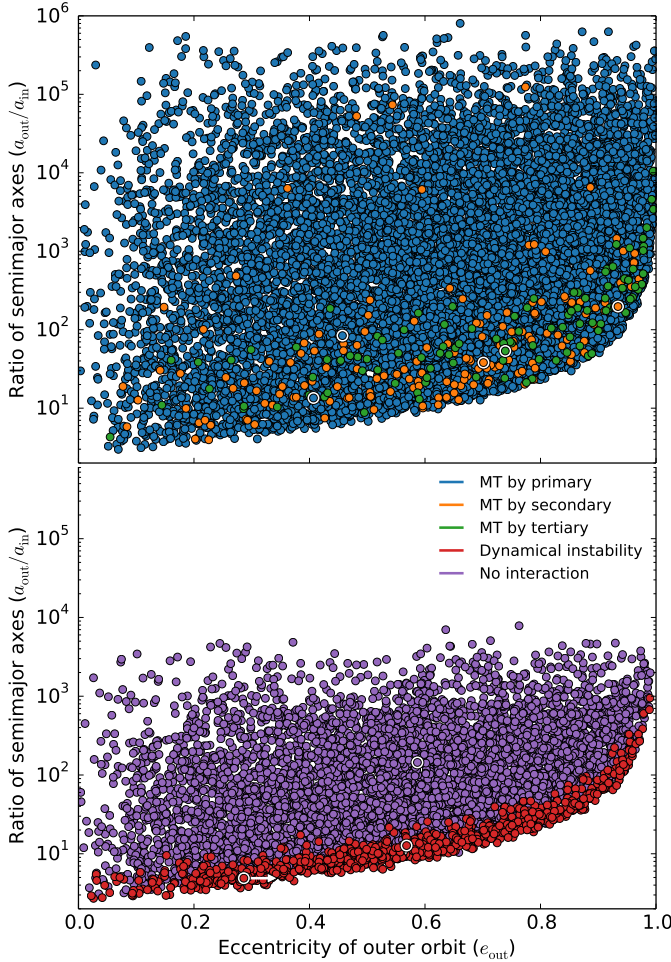
Fig. 7. Visualisation of the initial population of triples of the default model OBin, which highlights the different dynamical regimes as shown in Fig. 4. The examplary systems mentioned in the text are marked with white halos.

Fig. 8. Cumulative eccentricity distribution at the onset of mass transfer for the three different models normalised to unity (solid lines). The dashed lines represent the initial eccentricity distribution at ZAMS. The solid lines reflect those systems that are eccentric upon the first RLOF, which is about 40% of systems.

der Helm et al. 2016; Bobrick et al. 2017; Hamers & Dosopoulou 2019). Whereas tides act to circularise the orbit, enhanced mass loss at (or close to) periastron (either from stellar winds or RLOF) can enhance the eccentricity, such that some binaries can remain eccentric for long periods of time (Van Winckel et al. 1995; Soker 2000; Sepinsky et al. 2007b; Bonačić Marinović et al. 2008; Sepinsky et al. 2009; Vos et al. 2015; Dosopoulou & Kalogera 2016; Kashi & Soker 2018). Mass transfer in eccentric orbits is observationally supported by a number of eccentric semidetached and contact systems (Petrova & Orlov 1999; Boffin et al. 2014), systems close to RLOF (Gualandris et al. 2004; Raguzova & Popov 2005; Bonačić Marinović et al. 2008; Nicholls & Wood 2012; Walter et al. 2015).

Fig. 10 shows the evolutionary phase of the donor star at the onset of mass transfer. The most common donor stars are on the red giant branch (RGB, 50-52%), followed by the main-sequence (MS, 16-20%) and the asymptotic giant branch (AGB, 15-17%). Moreover, Fig. 10 shows that mass transfer in an eccentric orbit is most likely to occur with a fairly unevolved donor star (MS-RGB). In particular for donors on the MS and HG that have weak tides, the inner orbits are typically still eccentric upon mass transfer; in roughly 9 out of 10 cases.

These results also depend on the mass range of the donor star. For systems with relatively high primary masses, it is relatively
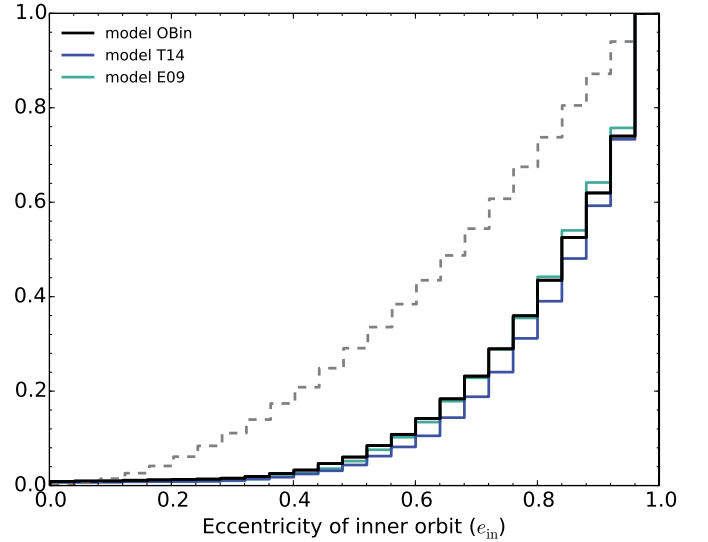
more common that the donor star is on the MS or HG gap upon Roche lobe overflow, and less common to be on the RGB. For example, while over 40% of MS donors have a high-mass origin (here $m_1 > 2M_\odot$), less than 15% of RGB donors are massive. Additionally, the eccentricity distribution is affected as well, because the tidal timescale of the star is linked to its mass and evolutionary state. For example, more massive MS stars have shorter tidal timescales, and therefore a larger fraction of systems are circularised upon mass transfer i.e. 12% for $m_1 > 2M_\odot$ versus 8.5% for $1.25M_\odot < m_1 < 2M_\odot$ for MS donors in model OBin. Even lower mass stars have convective envelopes and corresponding even shorter tidal timescales, such that 16% of systems are circularised. We note however, that the overall trend that mass transfer in an eccentric orbit is most likely to occur with a fairly unevolved donor star is robust against variations in the mass range in our simulations.

The interplay of LK cycles with tidal friction (LKCTF) can give rise to stellar migration (Mazeh & Shaham 1979; Kiseleva et al. 1998; Fabrycky & Tremaine 2007; Naoz & Fabrycky 2014; Liu et al. 2015; Bataille et al. 2018; Hamers 2019). During the high-eccentricity parts of the LK cycles, the inner stars pass each other at short periastron distances when tidal dissipation is very efficient. At this point the tides act to reduce the eccentricity as well as the semi-major axis of the inner orbit. LKCTF has been studied extensively for low-mass MS stars (for stellar triples as well as planetary systems), but a test of the efficiency for evolved stars is missing so far. We aim to quantify the importance of stellar migration for different stellar donors by studying the change in the semilatus rectum of the inner orbit ($a_p \equiv a_{in}(1 - e_{in}^2)$) from the initial to the final orbit, i.e. $\mathcal{A} \equiv a_{p,init}/a_{p,final}$ in Fig. 9. If a system would suffer from strong tidal circularisation (without stellar winds and LK oscillations), $\mathcal{A} = 1$. If instead the stellar wind mass losses are substantial, $\mathcal{A} < 1$, such as during the giant stages. If instead stellar migration occurs due to LKCTF, $\mathcal{A} > 1$. Fig. 9 shows a clear difference between different evolutionary states of the donor stars. Over 75% of systems with low-mass MS donors experience stellar migration (here $\mathcal{A} > 1.05$),
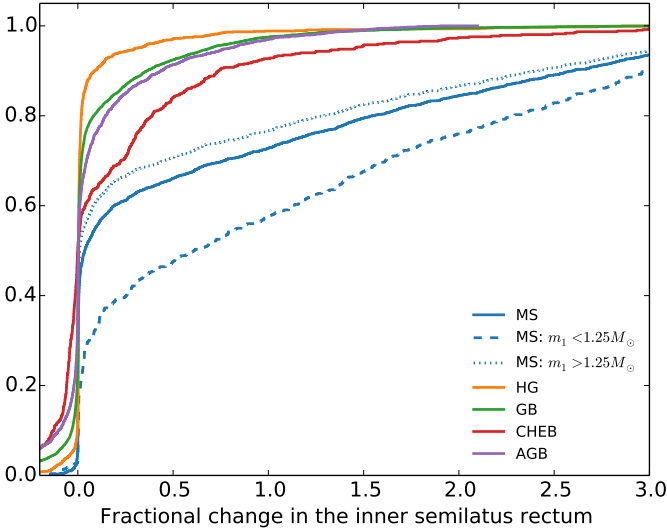
Fig. 9. How much does the semilatus rectum of the inner orbit ($a_{\rm p} \equiv a_{\rm in}(1 - e_{\rm in}^2)$) change between formation and the onset of mass transfer? The figure shows the cumulative distribution of the logarithm of $\mathscr{A} = a_{\rm p,init}/a_{\rm p,final}$ for model OBin, while other models show qualitatively similar behaviour. LK cycles with tidal friction drive the inner stars closer together ($\mathscr{A} > 1$), whereas stellar winds act to widen the orbit ($\mathscr{A} < 1$). The figure shows that LKCTF can shrink the inner orbit most efficiently for low-mass MS stars, followed by higher-mass MS stars, and evolved stars.
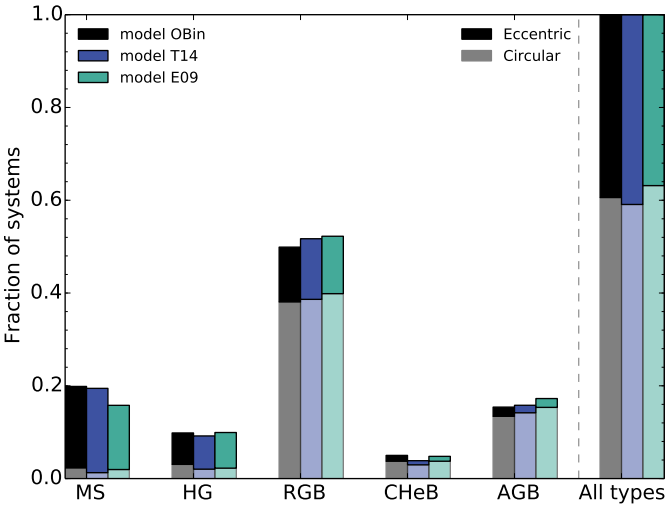

Fig. 10. Evolutionary states of the donor stars at the onset of mass transfer in circularised as well as eccentric orbits. The fractions are given with respect to the total number of systems where the primary fills its Roche lobe. Non-evolved donors predominantly initiate mass transfer in eccentric orbits and vice versa.

whereas this is over 40% for their higher-mass counterparts, and over 30% for evolved donors. The amount of orbital shrinkage ranges from a factor of a few for systems with evolved donors to several orders of magnitude for donors on the MS.

The delay times between the onset of the mass transfer and the formation of the triple range from several hundreds of Myr to many Gyr. We find a few percent of systems ($\lesssim 5\%$) that experience RLOF within 1Myr in this channel. For less than ~1% the mass transfer starts within 0.01Myr. These systems have strong
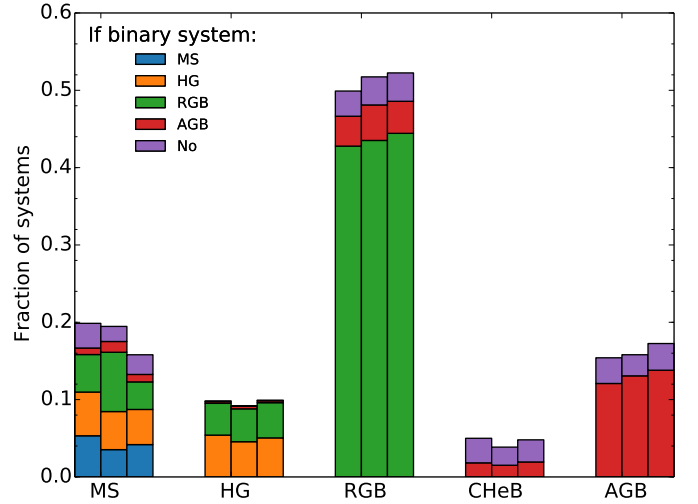

Fig. 11. Evolutionary states of the donor stars at the onset of mass transfer. For each type of donor star, three bars are shown, with the left representing model OBin, middle model T14, and on the right model E09, similar to Fig. 10. With colour we indicate when the donor star would initiate mass transfer if the inner binary would be isolated: from the bottom to the top, on the MS (blue), HG (yellow), RGB (green) or AGB (red), or if mass transfer happens at all (if not: purple). Overall, the onset of RLOF is expedited due to the presence of the tertiary star and the frequency of case A mass transfer increases by a factor 3.7-5.5.

LK cycles with comparable timescales and an inclination distribution that peaks around 90°. Although technically the systems are detached and dynamically stable at initiation according to Eq. 1, it is questionable whether these systems could have formed in the first place; very likely the stars would have had contact or strong tidal evolution during the pre-MS phase when the radii of the stars were larger.

3.1.1. Comparison to isolated binaries

In this section we study the role of the tertiary star for the systems where the primary initiates mass transfer. We study how these systems would evolve without the presence of the tertiary star. We take the inner binaries from model OBin, T14 and E09, remove the tertiary, and assume their orbits completely circularise before RLOF due to tides to the semilatus rectum. The stellar evolution, including winds and its effect on the orbits, is taken into account in the same way as in TRES.

Overall, we find that for the same binary, mass transfer will occur earlier in its evolution if the binary is orbited by a third body. As an example we mention the following system: $m_1 = 1.33 M_\odot$, $m_2 = 1.07 M_\odot$, $m_3 = 0.26 M_\odot$, $i = 71.5°$, $a_{\rm in} = 70.1 R_\odot$, $e_{\rm in} = 0.65$, $g_{\rm in} = -0.38$rad, $a_{\rm out} = 945 R_\odot$, $e_{\rm out} = 0.41$, $g_{\rm out} = -0.88$rad on the ZAMS. The system undergoes strong LK cycles with timescales of the order of a thousand years. The system is even in the eccentric LK regime as indicated by an octupole parameter of $\epsilon_{\rm oct} \approx 0.004$, and its location in Fig. 7. As the inner eccentricity increases from 0.65 to 0.94, the primary star fills its Roche lobe. This happens after 2.8Gyr when the primary star is still on the MS. Without the presence of the tertiary star, the eccentricity of the (previously inner) orbit would not increase, but rather decrease until circularisation is reached. At that point the orbital separation is about $40 R_\odot$. This is too large for the system to experience mass transfer when the

primary star is still on the MS. However afterwards, when the primary star has crossed the Hertzsprung gap and is ascending the giant branch, the primary star finally fills its Roche lobe.

Fig. 11 shows how often mass transfer is brought forward due to the presence of the tertiary star. For example, in 9.5-11% of isolated inner binaries the primary will fill its Roche lobe on the Hertzsprung gap. If the tertiary is taken into account, 47-52% of these systems will already interact when the donor star is still on the MS. However, the total fraction of HG donors in triples (9-10%) is roughly similar to that in binary systems, as binary systems with more evolved-donors (mostly on the RGB) experience mass transfer earlier when in a triple. Secondly, we note that in 3.9-5.0% of triples the primary star is a core-helium burning star at the onset of the mass transfer, whereas in intermediate-mass binaries we do not anticipate this to occur. The difference between binaries and triples is largest for MS donors. Whereas in intermediate-mass binaries, merely 3.5-5.3% experience case A mass transfer (Kippenhahn & Weigert 1990), for triples this increases to 15.8-19.9%. The majority of case A mass transfer in triples is brought about by three-body dynamics, which is also supported by their eccentricity distribution (Fig. 10).

In the experiment of removing the tertiary star from the inner binary, we also find that some inner binaries do not experience mass transfer without the tertiary. This is the case for 11-13% of the triples, with no preference for the evolutionary state of the donor star (Fig. 11). For the full populations of triples (not only the ones where the primary initiates a mass transfer phase), 65-77% of triples experience mass transfer, while this decreases to 58-70% when removing the tertiary. In conclusion, mass transfer can occur in 10% more systems in a triple population than if the inner binaries were isolated.

However, realistic isolated binaries have different orbits than the inner binaries of triples (see bottom panel of Fig. 3). To assess the frequency of mass transfer in binaries and the types of their donor stars, we construct two sets of initial binary populations. The models differ with respect to the distribution of orbital separations; an uniform distribution in the logarithm of the orbital separation between $5R_\odot$ to $5 \cdot 10^6 R_\odot$ (green dash-dotted curve in Fig. 3), or the log-normal distribution in periods described in Sect. 2.1 (black dotted curve in Fig. 3). The former and latter model are related to model OBin and T14 respectively, in which both a_{in} and a_{out} are drawn from the same distribution, but the requirement of dynamical stability skews the orbital distributions (Sect. 2.1). In our binary models the primary mass, secondary mass and eccentricity are distributed in a similar fashion as m_1, m_2, and e_{in}. In the population with the log-uniform distribution we find RLOF can take place in only 39% of systems, compared to 65% of triples in model OBin. Adopting the log-normal distribution, the fraction drops even further to 28%, whereas mass transfer occurs in 77% of triples in model T14. In conclusion, the tertiary star can drive inner binaries to RLOF, that would not have interacted without the tertiary present. This is partly because of the LK-cycles the tertiary can raise on the inner binary, but predominantly because the inner binaries are typically more compact than isolated binaries in order for the triple to be dynamically stable.

3.2. Mass transfer initiated by the secondary star

The second evolutionary channel involves mass transfer in the inner binary where the secondary star is the donor star. In contrast, in the previous section it was the primary star (i.e. the initially most massive star) that initiated the mass transfer event. In our simulations, 0.7-0.8% of triples experience mass transfer

initiated by the secondary star. This gives a Galactic event rate of about 3-4 times every 10^4 years. We differentiate between two scenarios; those where the primary star is still experiencing nuclear burning and those where the primary has become a WD at the onset of the mass transfer. The latter is slightly more common, comprising $53 - 61\%$ of the systems.

In the first scenario typically both the primary and the secondary are on the MS. Their masses are similar with a median mass ratio of more than 0.93. Though the secondary fills its Roche lobe, the primary is very close to Roche lobe overflow as well. Typically the radius of the primary is within a few percent of the associated Roche lobe. Likely the system will become a contact binary such that the difference between the primary and secondary star is an academic one. Additionally, there are systems for which the mass transfer starts within ~1Myr since formation. As discussed in Sect. 3.1, it is likely these systems would have interacted previously on the pre-MS. It comprises 42% of the systems in the first scenario. The fraction goes up to 61% for model T14.

In the second scenario the primary star has already evolved to the remnant stages without initiating mass transfer. When the secondary star fills its Roche lobe, mass is transferred to a compact object, such that cataclysmic variables and low-mass X-ray binaries could be formed in this way. Typically the mass transfer phase starts at late times i.e. several Gyrs after star formation. If the inner binary were to be isolated, the evolution of this second scenario would not be possible: if the orbit is wide enough such that the primary does not fill its Roche lobe during its evolution, the secondary star will not do so either[4]. The second scenario is possible for triples due to the interplay of three-body dynamics with other physical processes. Overall, this occurs in two different ways which are equally likely to occur:

- In one case, the inner orbit shrinks due to the interplay of LK cycles with tidal friction (i.e. LKCTF) as shown in Fig. 12. When the primary star is in the evolved stages of evolution, and close to RLOF, tides are efficient to circularise the inner orbit as well as reduce its semimajor axis, for example at ~ 3500 Myr and ~3650 Myr in Fig. 12. The contraction is counteracted by the mass loss in the stellar winds of the primary star (as seen at ~3650Myr). After the primary has become a WD, and the secondary star evolves, tides make the inner orbit contracts for the third time, and circularise. Ultimately this leads to mass transfer from the secondary star to the (primary) WD component at ~4100Myr. In this channel the secondary stars are typically evolved stars from the RGB to the AGB. For roughly half of the systems, the inner orbits reach complete circularisation.

- A different pathway of evolution is shown in Fig. 14. For this type of systems, the inner orbits have widened in response to the wind mass losses of the primary stars. The orbits are extremely eccentric at the moment of RLOF, on average $e_{in} \gtrsim 0.99$. At periastron, the stars pass at each other closely, but do not collide directly. The secondary stars are typically low-mass ($m_2 \lesssim 1M_\odot$) and on the MS. This type of system shows a rich variety of three-body dynamics. The octupole term of the three-body dynamics is relevant (i.e. $|\epsilon_{oct}| \gtrsim 0.001$) from the birth of the systems until the onset of the mass transfer[5]. An example evolution is shown in Fig. 14. It shows distinct modulations in the inner eccentricity and inclination both on short and long timescales that are

---

[4] This is strictly only true for low and intermediate mass stars, as for these stars the maximum radius attainable during the stellar life increases with the initial mass

[5] This is in contrast with the previous pathway in the second scenario. For those systems the octupole parameter has a median value of $(1 - 3) \cdot 10^{-4}$ initially and $(3 - 5) \cdot 10^{-4}$ at the onset of mass transfer,
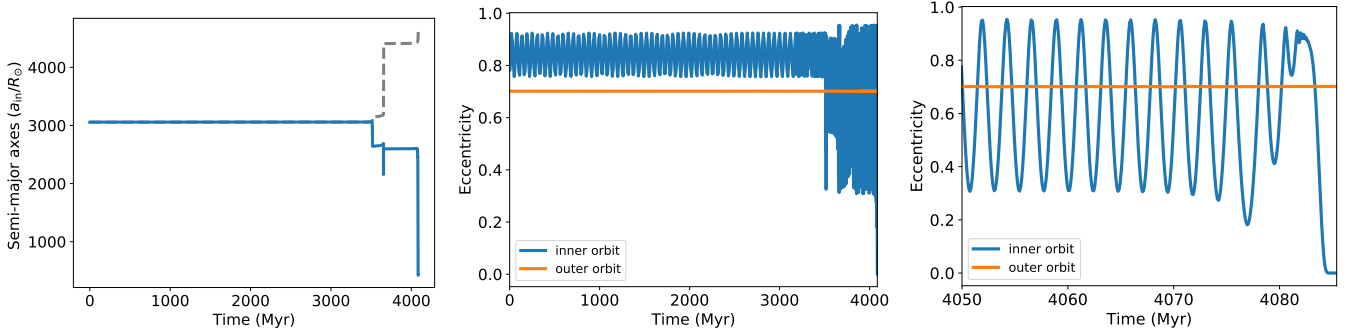
Fig. 12. First example of a system in which the secondary initiates the first mass transfer phase while the primary has already evolved to the WD stages. In this case the interplay between LK cycles, stellar evolution and tides shrinks the inner orbit in consecutive phases; when the primary evolves along the RGB at $\sim$ 3500 Myr, on the AGB at $\sim$3650 Myr, and when the secondary is on the RGB at $\sim$4100 Myr. The top and middle panel show the inner semimajor axis and eccentricity as a function of time. The bottom panel shows the circularisation of the inner orbit in the final stages before the mass transfer. In the top panel we have overplotted in dashed grey the widening of the inner orbit if only stellar winds would act upon it. The initial conditions of this system are: $m_1 = 1.42 M_\odot$, $m_2 = 1.36 M_\odot$, $m_3 = 0.70 M_\odot$, $i = 70.9°$, $a_{in} = 3057 R_\odot$, $e_{in} = 0.86$, $g_{in} = 1.30$rad, $a_{out} = 116551 R_\odot$, $e_{out} = 0.70$, $g_{out} = -1.99$rad.

linked to the quadrupole and octupole term, respectively. As the primary star evolves off of the MS, it loses mass in its stellar wind, most strongly at an age of 1900Myr. In response the orbits widen. The relative change in the inner orbit is larger than that of the outer orbit, such that the ratio a_{out}/a_{in} reduces. The octupole parameter increases slightly (in absolute terms) and the LK timescale shortens. At the same time (additional) apsidal motion from general relativity, tidal bulges and rotation is reduced. As these terms suppress the LK cycles, reducing the additional apsidal motion allows for stronger LK cycles. With this new configuration, the higher inner eccentricities can be reached that lead to the mass transfer event. In the case of Fig. 14, the mass transfer is preceded by orbital flips, from retrograde to prograde motion and vice versa (Lithwick & Naoz 2011; Katz et al. 2011; Teyssandier et al. 2013; Li et al. 2014).

The evolution in Fig. 14 is reminiscent of, but alternative to the mass-loss induced eccentric Kozai (MIEK, Shappee & Thompson 2013; Michaely & Perets 2014). In the MIEK-picture, a triple goes from the quadrupole regime to the octupole regime, and the transfer is a consequence of the change in masses of the stellar components. Typically our systems are in the octupole regime from birth onwards (see also Fig. 7), but the effect of the octupole term is amplified (or less repressed) due to mass loss and its effect on the orbits.

Classical MIEK-behaviour where the triples move from the quadrupole to the octupole regime is uncommon in our simulations. In all models combined, we have only encountered four such systems. The prototype of classical MIEK-behaviour (Shappee & Thompson 2013; Michaely & Perets 2014) is a triple with initially roughly equal mass stellar components, but a large inner mass ratio after the one of the inner stars has become a WD, such that the magnitude of the octupole parameter considerably increases. This phenomenon is uncommon due to the prevalence of low-mass stars in the IMF that do not lose much mass in their winds. We expect MIEK-behaviour to be more likely for more massive stars. Note though that very massive stars can undergo a supernova explosion with accompanying natal kick, which also drastically changes the dynamical regime of the triple, often leading to a disruption of the system (Pijloo et al. 2012; Lu & Naoz 2019).

The systems of the second scenario occupy a specific region of phase space on the ZAMS, that is the upper right corner of Fig. 13. As the evolution involves stars that evolve to or through the giant phases, the inner orbits are relatively wide ($a_{in}(1 - e_{in}^2) \gtrsim$ few100$R_\odot$). The outer orbits are not extremely close to the inner orbit (to ensure dynamical stability), nor are they extremely wide (to ensure that three-body dynamics are relevant on the evolutionary timescale of the stars). The systems of the first scenario (with components on the MS at the onset of mass transfer) can be found predominantly in the bottom left corner of Fig. 13 with ($a_{out}(1 - e_{out}^2) \lesssim 10^3 - 10^4 R_\odot$).

3.3. Mass transfer initiated by the tertiary star

The systems in this channel occupy a specific region of phase space (Fig. 7 and 13). Both the inner and the outer orbits are small, such that the tertiary star can fill its Roche lobe. The ratios of the inner and outer semimajor axis are smaller than for those systems where the primary fills its Roche lobe. While this could lead to strong three-body effect, LK cycles are not prominent. This can also be seen in Fig. 15 where the systems in this channel avoid inclinations around 90°. If LK cycles were to be important, it would likely lead to mass transfer in the inner binary before the outer star experiences RLOF[6].

In our study the tertiary star initiates a mass transfer phase in 0.9-1.1% of triples with an intermediate mass primary. The rate decreases to 0.6% for model OBin as fewer binaries have short outer orbital periods. Our results are consistent with observational estimates. de Vries et al. (2014) estimated that out of 725 triples in the Tokovinin catalogue of multiple stellar systems in the Solar neighbourhood (Tokovinin 2010), 6 systems ($\approx$ 1%) would experience mass transfer initiated by the outer star.

We find that initially the tertiary star is more massive than the primary or the secondary star, such that it evolves on a shorter timescale. Typically the donor stars are evolved stars with the far majority of them on the AGB (74-87%). This is also in agree-

---

which is significantly below where the octupole terms are expected to be important.

[6] See for instance the example given in section 3.1 with initial masses $m_1 = 1.63 M_\odot$ and $m_3 = 2.06 M_\odot$. Even though $m_1 < m_3$, such that the stellar evolution timescale of the primary is longer than that of the tertiary, the primary is the first star to fill the Roche lobe, not due to its expansion in radius, but due to the reduction in the instantenous Roche lobe.
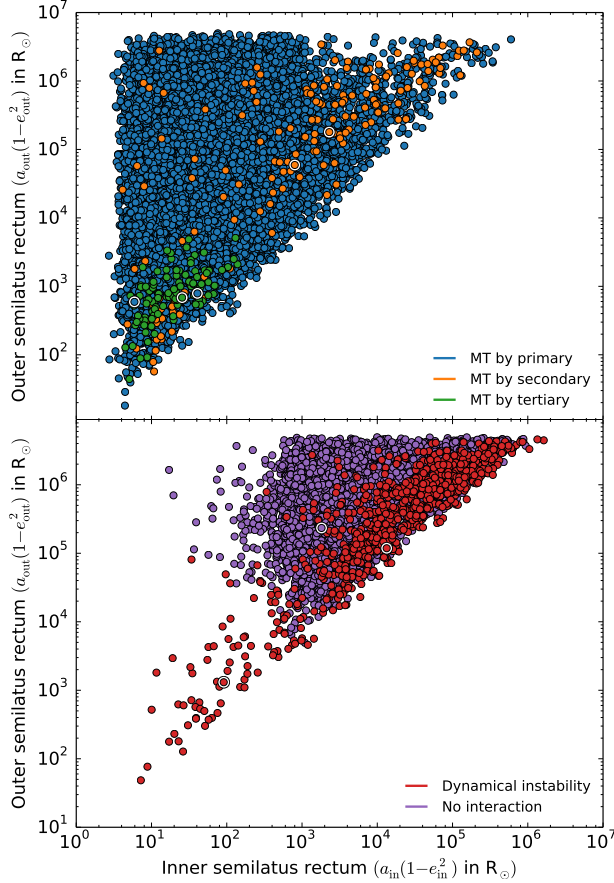
Fig. 13. The most common evolutionary channels occupy different areas of initial phase space. The x- and and y-axes show the distance the inner and outer orbit would circularise to if tides were efficient. The examplary systems mentioned in the text are marked with white halos.

ment with the findings of de Vries et al. (2014). The primary and secondary are typically still on the MS.

The tertiary star is typically less massive than the primary and secondary star combined. In model OBin and Tok14 this is by construction. In model E09, it is the case for 58% of the systems in this channel. This fraction is set by the initial mass ratio distribution, as well as by stellar winds that strip the envelopes of the evolved tertiary stars.

For 67% of triples in model OBin and model T14 the outer orbit has circularised (i.e. $e_{out} < 10^{-3}$) at the onset of mass transfer. For model E09 this fraction is lower (i.e. 46%), but still significant. The systems that maintain eccentric outer orbits upon mass transfer, tend to have high eccentricities with median values between 0.8-0.9. Note that regarding the tides raised on the tertiary star, we assume the inner binary is a point particle. If the tidal perturbation of the tertiary by the (extended) inner binary is efficient (i.e. tertiary tides), it may lead to a contraction of the inner binary and subsequent RLOF or mergers before the tertiary fills the Roche lobe (Gao et al. 2018).

A representative example from this channel is the following system: $m_1 = 1.92M_\odot$, $m_2 = 1.47M_\odot$, $m_3 = 2.09M_\odot$, $i = 155°$, $a_{in} = 28.1R_\odot$, $e_{in} = 0.30$, $g_{in} = -0.39$rad, $a_{out} = 1507R_\odot$, $e_{out} = 0.74$, $g_{out} = -1.79$rad on the ZAMS, see also Figs. 7 and 13. As the tertiary is more massive than the primary and secondary, it evolves off the MS first. It fills its Roche lobe as an AGB star

after 1.32 Gyr. At that time the inner orbit has only changed slightly ($a_{in} = 27.6R_\odot$, $e_{in} = 0.29$), however the outer orbit has become circularised. In the absense of stellar winds the outer semi-major axis would have been $a_{in}(1 - e_{in}^2) = 681R_\odot$, however due to 1.3% mass loss from the tertiary the final orbit is $a_{out} = 690R_\odot$.

Next, we explore the outlook of the mass transfer phase. Is the mass transfer phase dynamically stable or unstable? Whereas stable mass transfer in binaries persists on long timescales (e.g. the thermal or nuclear timescale of the donor star), unstable mass transfer occurs on short (dynamical) timescales (i.e. common envelope (CE) evolution), and is expected to lead to orbital contraction and often a merger of the stars. To quantify the stability, we construct the following simple picture. We replace the inner binary with a point particle of the same total mass, we assume the tertiary star has deep surface convection zones, and we assume that the mass transfer is conservative. With these assumptions unstable mass transfer can be avoided if the mass ratio is below a critical mass ratio for which we adopt Eq.57 of Hurley et al. (2002). Where isolated binaries with evolved donor stars are typically expected to undergo a CE-phase (see e.g. Toonen et al. 2014), in this triple channel a common-envelope phase can be avoided for 29-43% of systems. We stress that our quantification of the stability is a crude model that does not take into account the eccentricity of the orbit, but it suggests that stable mass transfer is more readily achieved in these systems, because the tertiary star is typically less massive than the inner binary (while more massive than the other stars individually).

Subsequently we consider what happens to the material if it flows from the tertiary through the first Lagrangian point towards the inner binary. Will the material hit the inner binary directly or will the stream intersect itself and form an accretion disk around the inner binary? In our systems the classical circularisation radius (See section 4.5 and Eq.4.20 in Frank et al. 2002) of the material is typically 10-20% of the outer orbit. When taking into account that an eccentric orbit has less angular momentum by a factor $\sqrt{(1 - e_{out}^2)}$, the expected circularisation radius R_{circ} would be smaller by a factor of a few for those orbits. Typically, we find that the inner binaries are of comparable size to the circularisation radius. We find that only for 11-33% of systems the inner apocenter is well within the circularisation radius ($a_{a,in} \equiv a_{in}(1 + e_{in}) < 0.1R_{circ}$), such that an accretion disk would form (Fig. 16). If the proximity of the tertiary star induces or amplifies the LK cycles and inner eccentricity variations, the fraction of system with accretion disk reduces further.

How does the stream of material effect the inner binary? The onset of mass transfer from a tertiary to an inner binary has been simulated by de Vries et al. (2014) for two observed systems, Tau and HD 97131 using a combination of stellar evolution, gravitational dynamics and hydrodynamics. In their simulations, de Vries et al. (2014) finds that an accretion disk is not formed, consistent with our expectations of the triple population. The accretion stream intersect with the orbit of the inner binary and interacts with the stellar companions. A small amount of material is accreted by the stars of the binary, but the majority is ejected from the inner binary. The inner orbital separation shrinks and may ultimately lead to mass transfer in the inner binary itself. The evolution of the mass transfer phase and the dynamical consequences are outside of the scope of the current study (but see Portegies Zwart & Leigh 2019, in the context of twin blue stragglers).
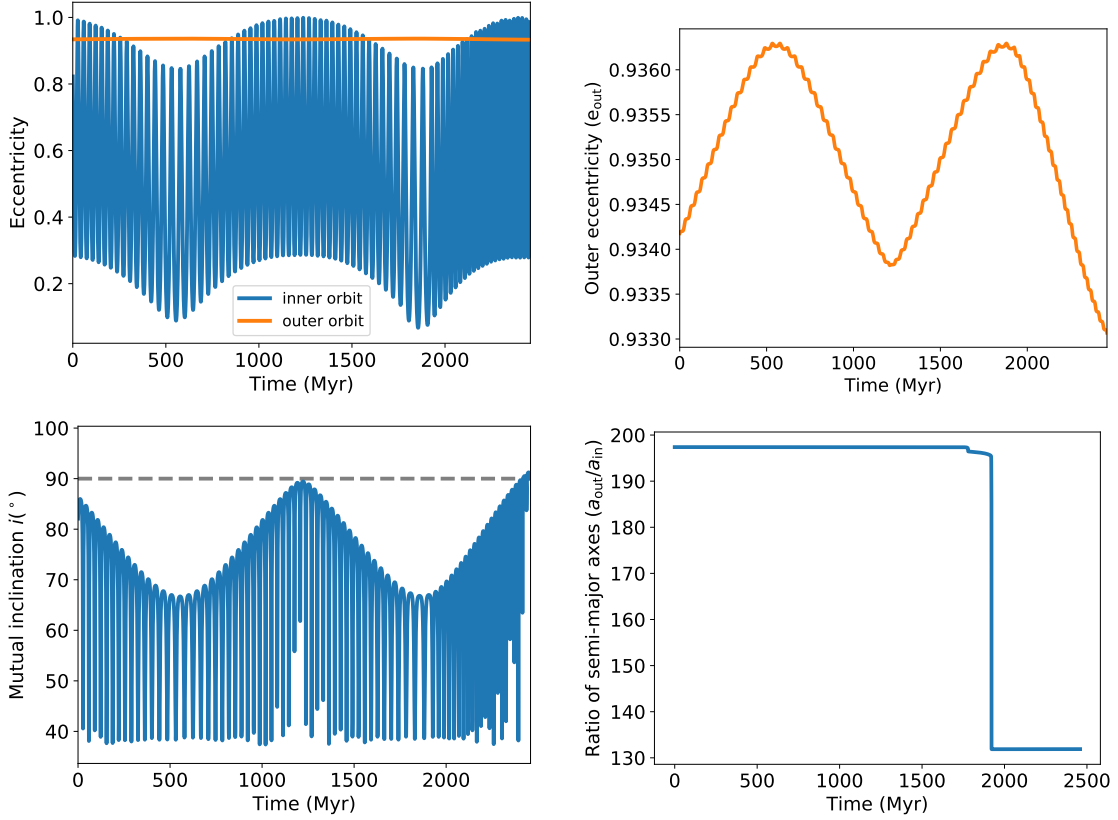
Fig. 14. Second example of a system in which the secondary initiates the first mass transfer phase while the primary has already evolved to the WD stages. Here the interplay between the different terms of the three-body dynamics effects and stellar evolution makes the inner orbit extremely eccentric, leading to the mass transfer phase. The top two panels show the eccentricities as a function of time, followed by the inclination and the ratio of the outer to inner semimajor axis as a function of time. The short and long term modulations seen in these figures represent the timescales of the quadrupole and octupole terms, respectively. After the primary has become a WD at ~1900Myr, and the inner and outer orbit have approached each other, the system experiences a flip in the orbital inclination (when crossing the black dashed line of $i = 90°$), accompanied by an extreme eccentricity in the inner orbit and a subsequent mass transfer event. The initial conditions of this system are: $m_1 = 1.76M_\odot$, $m_2 = 0.26M_\odot$, $m_3 = 1.22M_\odot$, $i = 82.1°$, $a_{in} = 7123R_\odot$, $e_{in} = 0.82$, $g_{in} = -0.63$rad, $a_{out} = 1406013R_\odot$, $e_{out} = 0.93$, $g_{out} = -1.12$rad.

3.4. Dynamical instability

One of the possible outcomes is a dynamical instability induced by the tertiary, i.e. triple evolution dynamical instability (TEDI); initially the triple is dynamically stable, but as the triple evolves it crosses the stability limit (Eq. 1). The subsequent evolution is reminiscent of that of interactions between a binary and a single star in stellar clusters. It can give rise to close encounters between the stars, a collision, a compact binary, or a dissolution of the triple in to a binary+single star or three single stars for example. This process was also used to explain the great eruption of Eta Carinae (Portegies Zwart & van den Heuvel 2016).

The systems that go through a TEDI are found in a specific region of initial phase space (Fig. 13). The initial ratio of outer to inner semilatus rectrum is small, such that the systems are already close to the stability limit at birth. As a result, they are typically in the eccentric LK regime (Fig. 7), with $|\epsilon_{oct}| > 0.01$ for 75-80% of TEDI triples and $|\epsilon_{oct}| > 0.001$ for over 97%. However, the initial inclinations of the systems are biased away from inclinations around 90° to avoid mass transfer in the inner binary (Fig. 15), similar to the previous channel where the tertiary fills its Roche lobe.

The TEDI occurs in 2.3-2.5% of all triples in model T14 and E09, and 4.2% in model OBin. The birthrate in model OBin

is increased as there are more systems with wide inner orbits initially ($a_{in} \gtrsim 10^3R_\odot$).

We differentiate between two scenarios. In the first scenario the dynamical instability occurs when all stars are still on the MS. The system goes through many LK cycles (of the order of tenths to thousands of cycles on average). Due to the higher-order terms in the secular approximation, the outer eccentricity increases until the system crosses the stability limit. In Fig. 4 the system would move horizontally towards higher outer eccentricities. In the second scenario, the primary star has moved of the MS. During the giant stages of evolution, the primary star suffers strong mass losses through stellar winds. Assuming an adiabatic effect on the orbit, the orbit widens in response to the mass loss. The relative amount of orbital widening is proportional to the relative amount of mass loss. This means that the inner orbit widens more relatively, approaches the outer orbit, and the system as a whole can become unstable (Kiseleva et al. 1994; Iben & Tutukov 1999; Perets & Kratter 2012). In Fig. 4 the system would move vertically downwards. At the moment of the TEDI, the primary is typically an evolved star. For 62-64% of systems the primary is on the AGB. In 24-31% of systems, the primary has already become a WD, and the systems becomes unstable due to the stellar winds that acted on the orbit as well as enhanced the importance of the octupole terms.
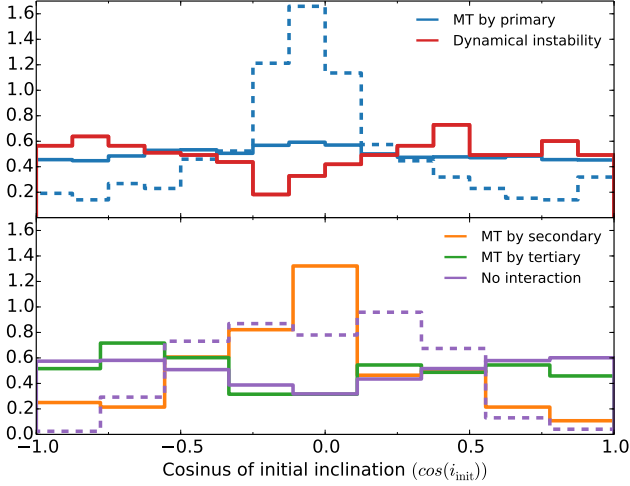
13

Fig. 15. The initial distribution of inclinations of the different channels normalised to unity. Systems in which the primary initiates a mass transfer phase (blue) show no strong bias towards a certain inclination, however, the subset with wide initial orbits ($a_{in} > 5000R_\odot$) that would not experience mass transfer without the presence of the tertiary are biased towards high initial inclinations. Systems in which the secondary initiates a mass transfer phase (orange) are preferentially found at high inclination, whereas systems in which the tertiary initiates mass transfer (green) or there is no mass transfer (purple) preferentially avoid high inclinations. The subsection of the latter that experiences LKCTF are shown as the dashed purple line. The figure is based on model OBin. Model T14 and E09 have similar distributions.

The systems in the second scenario have initial orbital separations of $a_{in}(1 - e_{in}^2) \gtrsim 10^3 R_\odot$ (Fig. 13). Systems evolving through the first scenario have initial semilatus recti that extend to smaller values. An example of this evolution is marked in Figs. 7 and 13. The initial conditions are $m_1 = 1.25M_\odot$, $m_2 = 0.52M_\odot$, $m_3 = 0.57M_\odot$, $i = 75.4°$, $a_{in} = 291R_\odot$, $e_{in} = 0.83$, $g_{in} = -0.93$rad, $a_{out} = 1427R_\odot$, $e_{out} = 0.29$, $g_{out} = 1.73$rad. At birth the system is close to the stability limit, and crosses it after 181Myr. On this timescale the stars do not loose any mass to the stellar winds. With an LK timescale of 379yr, the system has undergone thousands of LK cycles before crossing the stability boundary. The system becomes dynamically unstable as the outer eccentricity increases from the initial 0.29 to 0.34 due to interactions with the tertiary star (indicated by the arrow in Fig. 7). The system is well inside the octupole regime with an octupole parameter of 0.026-0.031.

Figs. 7 and 13 also show an example of the second scenario (with initial parameters $m_1 = 2.72M_\odot$, $m_2 = 0.59M_\odot$, $m_3 = 1.29M_\odot$, $i = 6.2°$, $a_{in} = 13760R_\odot$, $e_{in} = 0.18$, $g_{in} = 0.68$rad, $a_{out} = 174881R_\odot$, $e_{out} = 0.57$, $g_{out} = -0.51$rad). As the primary star evolves and ascends the AGB, it loses mass to stellar winds. After 632 Myr, the primary has lost 45% of its mass and the system crosses the stability limit. Due to the wind mass loss, the inner orbit has widened more than the outer orbit with factors 1.58 and 1.36 respectively. The system moves vertically downwards in Fig. 7 by 14%. This is within the size of the marker.

The fraction of systems with unevolved primaries is highest in model T14 and E09 (56% and 50% respectively) compared to model OBin (37%), as there are more orbits that are compact initially in model T14 and E09. When the system becomes un-
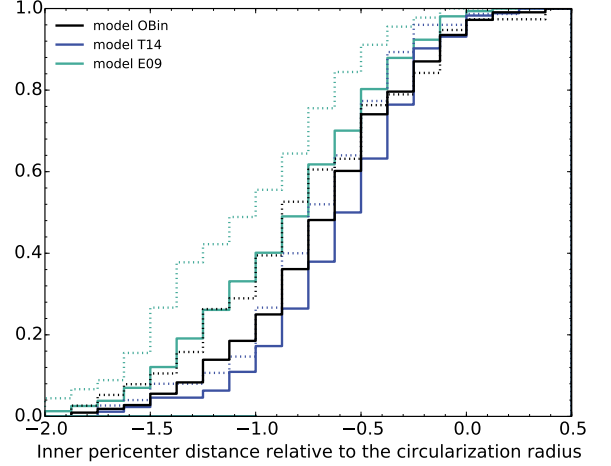
Fig. 16. Is there enough room in the system for an accretion disk to form around the inner binary when the tertiary fills its Roche lobe? The figure shows the ratios of the apocenter distance of the inner two stars to the expected circularisation radius of the inflowing material, i.e. $a_{in}(1 + e_{in})/R_{circ}$. The dashed lines represent the distribution for the subset of systems for which we expect the mass transfer from the tertiary towards the inner binary to occur in a stable manner. The distribution is normalised to unity.

stable, the secondary and tertiary are typically still on the MS in both scenarios.

We find an galactic TEDI rate of 1-2 per 1000 years, which is in agreement with the estimates of Perets & Kratter (2012) (4-6 per 1000 years) and Hamers et al. (2013) (0.4-0.75 per 1000 years). The former is based on a hybrid method combining analytical estimates with triple population synthesis excluding LK effects, and the latter is based on a population synthesis study of wide triples. Furthermore, Perets & Kratter (2012) simulate the further evolution of the triple, and show that for roughly a third of the systems destabilise on a short timescale (0.5Myr), and subsequently 10% of systems experience a collision between two of the stars of the triple. The stellar collision rate from destabilising isolated triples is an order of magnitude higher than that due to random encounters in Galactic globular clusters.

3.5. Survival for a Hubble time

In this evolutionary channel the systems stay intact for a Hubble time without experiencing RLOF and without becoming dynamically unstable. In the mass range considered in this study, the primary stars become WDs within a Hubble time. This channel is the second most common pathway for triples. About 27-30% of triples evolve this way in model OBin and E09, and 20% for model T14. The channel is less likely in model T14, as the average orbit tend to be more compact compared to the other models, making it harder to avoid RLOF (see also Fig. 3).

The systems of the current channel have wide inner and outer orbits (Fig. 13). Initially the outer orbits $a_{out}(1 - e_{out}^2) \gtrsim 10^5 R_\odot$. The median size of the outer orbit varies between the models, as they are closely linked to the initial distribution of orbits (see also Fig. 3). Initially the inner orbits range from $a_{in}(1 - e_{in}^2) \approx 500 - 10^5 R_\odot$ and peak around $2000 - 4000R_\odot$. RLOF is avoided by definition in this channel.

A representative example of a system in this channel is marked in Figs. 7 and 13. On the ZAMS it has the following parameters: $m_1 = 1.60 M_\odot$, $m_2 = 0.75 M_\odot$, $m_3 = 1.07 M_\odot$, $i = 16°$, $a_{in} = 2472 R_\odot$, $e_{in} = 0.51$, $g_{in} = 0.25$ rad, $a_{out} = 356776 R_\odot$, $e_{out} = 0.59$, $g_{out} = 1.55$ rad. In this system, the primary evolves off the MS first, sheds its envelope during the giant phases, and becomes a WD around $2.5 Gyr$. It this point the inner and outer orbits have widened to $4058 R_\odot$ and $506771 R_\odot$, respectively. Subsequently the tertiary evolves and becomes a WD around $9.8 Gyr$. As we assume the mass lost from the tertiary does not interact with the inner orbit, only the outer orbit is affected, and it widens to $654756 R_\odot$. The secondary star is of sufficiently low-mass to not evolve off the MS in a Hubble time. And thus, at the end of the simulation this sytem consists of a wide WD-MS binary which is orbited by a second WD.

Observational counterparts of this channel are the WD systems WD0413-07 (40 Eridani) and WD 2351-335 (Wegner & McMahan 1988; Scholz et al. 2004; Farihi et al. 2005; Tokovinin 2008; Toonen et al. 2017). 40 Eridani B is one of the closest WDs to us (e.g. Hollands et al. 2018). It has a M-dwarf companion in an orbit of 11.9" and a K-star companion in a wider orbit of 83.4". WD 2351-335 has two M-dwarf companions at 6.6" and 103" respectively.

Such systems with a single WD in the inner binary are relatively common in our simulations; 20-30% of systems in this channel. In 7-11% the secondary star becomes a WD as well and a wide double white dwarf binary is formed. For 30-41% of systems only the primary and the tertiary star becomes WDs. This option is more common in model E09, as more tertiaries are initially massive enough to form a WD within a Hubble time (Fig. 1). Lastly, 29-33% of systems in all models from a wide triple WD, as recently observed for the first time by Perpinyà-Vallès et al. (2019).

As the stellar components evolve from the ZAMS to the remnant stages, their orbits change due to mass loss from stellar winds. Assuming mass loss occurs adiabatically, the orbits widen (Sect. 2.2). In our simulations the outer orbit widens within a factor ∼5 typically. Many inner orbits widen as well, however a reduction of the inner orbit is also possible due to LKCTF. In 11-13% of systems in this channel the semilatus rectum of the inner orbit has decreased after a Hubble time, and 6-7% reach complete circularisation.

The initial distribution of inclinations is shown in Fig 15. Initial inclinations around 90° are avoided, as strong LK cycles would lead to RLOF. The systems that experience LKCTF-like behaviour and inner orbital shrinkage, are preferentially born at initial inclinations closer to 90° (purple dashed line in Fig. 15). Their inclinations oscillate and typically freeze-out around $40 − 50°$ and $130 − 140°$ (see also Fabrycky & Tremaine 2007; Naoz & Fabrycky 2014, for low-mass stellar triples)

4. Discussion

In this study we have stellar triples by modelling their evolution in a comprehensive way. That is we take into account both stellar evolution as well as three-body dynamics, and include the effects of tides and stellar wind mass losses. Here, we critically discuss the main assumptions that we did not vary in out modelling, and their effects on triple evolution.

Distribution of initial inclinations: In this study we have assumed an uniform distribution in the cosine of the inclination. Observationally, this is a good approximation for outer projected

separations[7] that are $\gtrsim 10^5 R_\odot$. However, at $\lesssim 10^4 R_\odot$ orbits are more aligned (Tokovinin 2017). This represents about 10% of systems in model OBin and E09, and about 20% in T14. It corresponds to the evolutionary channels where either the primary or the tertiary fills its Roche lobe (Fig. 13), where the latter preferably occurs in less inclined systems. Therefore, if we would incorporate the orbital alignment in triples with compact outer orbits, we expect that tertiary will be able to fill its Roche lobe in an even larger fraction of triples.

Distribution of initial eccentricities: In our models we have assumed that the initial eccentricities are distributed thermally ($f(e) \propto 2e$). There are observational indications that the distribution is flatter (e.g. Tokovinin & Kiyaeva 2016; Moe & Di Stefano 2017). In the absense of three-body dynamics, the effect would be similar to that of taking a different distribution of orbital separations that is biased towards wider orbits. This would reduce the number of systems in which the primary or tertiary fills its Roche lobe (Fig. 13). Regarding three-body dynamics, we expect some differences as well. If the outer eccentricities are smaller on average, one would move to the left in Fig. 4. The minimum a_{out}/a_{in} while preserving dynamical stability decreases. This would enhance the number of systems where the tertiary fills the Roche lobe. Also the parameter space of the standard LK regime is larger, and the LK-timescales themselves are longer as well, which means there would be more triples that do not interact and stay intact for a Hubble time. The LK cycles would be effected further through their dependence on the initial inner eccentricity. For initially circularised inner orbits in the test-particle approximation, LK cycles can only take place when the inclination is between 39.2-140.8° with a maximum eccentricity given by Eq. 3. For non-zero eccentricities, the parameter space widens in which LK cycles take place, and higher maximum eccentricies can be reached (depending on the initial eccentricity and the argument of pericenter). If the initial inner eccentricities are smaller on average, the occurence of LK cycles and their amplitudes is likely reduced.

Distribution of initial mass ratios: In model OBin & T14, we have adopted a simple formalism for the mass ratio distribution based on a first-order approximation to observations. This formalism consists of a uniform mass ratio distribution for the inner and outer mass ratios. The modelling of (Eggleton 2009) includes a populations of 'twins', that is near-equal-mass pairs, for compact orbits ($P < 25d$). They make up 25% of the population of compact binaries. This does not strongly affect how many triples experience mass transfer, but it does affect the subsequent mass transfer phase (for example the stability of the mass transfer and the orbital evolution).

There are also indications that the mass ratio distributions in wide binaries deviate from the uniform mass ratio distributions that are observed in more compact systems (e.g. Moe & Di Stefano 2017). The distributions for wide binaries would include more smaller companion masses than given by a uniform mass ratio distribution. A detailed study on the effect of this for triple evolution is beyond the scope of the current study, but our expectations are the following: First, fewer tertiaries would evolve off the main-sequence in a Hubble time. Therefore, naively, one would expect also fewer tertiaries to fill their Roche lobe. However, the systems in which the tertiary fills

---

[7] We note that on average the difference between the projected separation and the semi-major axis of the orbit is small. Assuming an average sky inclination of 60° (from a random distribution on the sky), and an average eccentricity of 2/3 (from the thermal distribution), the projected separation is 78% of the semi-major axis.

its Roche lobe have compact orbits initially, and therefore the occurrence rate of mass transfer that is initiated by the tertiary are likely well approximated in this work. Secondly, if the tertiary mass decreases (and other parameters stay the same), the LK timescales would increase, and the dynamical impact of the tertairy on the inner binary would decrease. In a previous study using the same code TRES (Toonen et al. 2018b) which focused on wide triples ($a_{in}(1 - e_{in}^2) > 2500R_\odot$) in a similar mass range ($m_1, m_2, m_3 < 7.7M_\odot$; $m_1, m_2 > 0.95M_\odot$), we varied the mass ratio distributions of the inner and outer orbits. Under the extreme assumption that the tertiary mass in uncorrelated to the mass of the inner two stars (i.e. drawn from a Kroupa-IMF), the fraction of systems undergoing mass transfer slightly decreased from 10-12% (their model Q_OUT) to 9.3-9.9% (their model STD).

Tidal evolution: Our simulations are based on a single set of assumptions for tidal interactions and their timescales, which affect the average eccentricities upon RLOF and the degree of orbital shrinkage during LKCTF. We note that our modelling is based on the classical equilibrium-tide model Hut (1981), which may not be appropriate for inner orbits with large eccentricities ($e_{in} \gtrsim 0.8$) and small periastron distances ($\lesssim 5R_\star$). In this regime, tidal energy dissipation occurs solely near periastron, where as in the equilibrium-tide model it is averaged over the entire orbit. Tidal energy dissipations is dominated by non-radial dynamical oscillations in stead, which are more efficient by orders of magnitude (e.g. Press & Teukolsky 1977; McMillan 1986; Kochanek 1992; Mardling 1995). The transition between the two regimes occurs near $e \approx 0.8$ (Mardling 1995). The highly eccentric inner orbits of triples are expected to decay to smaller eccentricities ($\approx 0.6 - 0.8$) at roughly constant periastron distance (Mardling 1995; Moe & Kratter 2018). As the instanteneous Roche lobe of a star is roughly proportional to the periastron distance (Eggleton 1983; Sepinsky et al. 2007a), the time of RLOF is likely not affected much. The inner orbit would be somewhat smaller and less eccentric.

Stellar winds: In the current study we have made simplifying assumptions regarding the stellar winds; we assume that stars loose mass in fast, spherically symmetric winds and that the wind matter is not accreted by any of the companion stars. The former is a common assumption in binary population synthesis studies (see e.g. the appendix of Toonen et al. 2014, for an overview), the latter is a simplification we have adopted in the current study. It mostly affects systems in the last three channels, as intermediate mass stars mostly suffer from stellar winds in the late stages of their evolution.

If the wind matter forms a more or less uniform medium around the system, one would expect Bondi-Hoyle-Littleton accretion (Bondi & Hoyle 1944) to take place. The amount of accretion on a stellar companion from the wind depends on the orbital parameters, the wind mass rate and wind velocity of the mass-losing star. By ignoring the possibility of wind accretion in this work, our simulations underestimate the companion masses up a few percents and overestimate the orbital separations accordingly. If the wind and orbital velocities are comparable in magnitude, the assumption of spherical symmetry is violated. In this case the wind can be focused and accreted on to the companion star with an enhanced efficiency and a possible contraction of the orbit (e.g. Mohamed & Podsiadlowski 2007; Saladino et al. 2018; Chen et al. 2019). Furthermore, Comerford et al. (2019) showed that the efficiency of wind accretion from a tertiary star onto the stars in the inner binary may be enhanced up to a factor two compared to the case where the secondary star was removed. We defer a more detailed investigation of the potential effects of wind accretion to a future paper.

Numerical stability: We note that in a few cases our numerical solver was unable to find a solution for the dynamical evolution of the systems. It concerns 0.35% of systems in model OBin, 0.65% for model T14, and 0.13% for model E09. The systems are compact with outer semilatus rectum smaller than a few thousand solar radii (bottom left in Fig. 13). The primary star is close to filling its Roche lobe, such that the tidal torques are strong. The systems have short LK timescales (i.e. $\lesssim 10^4$yr) compared to a Hubble time or the stellar lifetimes, and as such will undergo numerous LK cycles. Higher-order terms of the secular approximation are important for their evolution as well, that is $\epsilon_{oct} \gtrsim 0.001 - 0.01$.

5. Conclusions

In this paper we aim to provide a systematic exploration of the evolution of stellar triples. We focus on the long-term evolution of isolated and hierarchical triples with low- and intermediate mass stars. The evolution of these systems are governed by stellar evolution, three-body dynamics, and dissipative processes such as tides and stellar winds. For a review of the relevant processes see Toonen et al. (2016). The expected birth rate of these triples is ~ 5 per decade, and ~ 50 per decade in the full mass range.

We find that in the majority of triples, the stars will interact with each other during their lifetime (Tbl. 2, Fig. 6). This can be either dynamically (through disruptions of the systems, or modifications to the stellar orbits) or physically (through mass transfer, mergers or collisions). Typically the initially most massive star in the inner binary fills its Roche lobe and starts transferring mass to its companion(s). This happens in 63-74% of triples in our samples depending on the model. A few percent of triples (2-4.5%) becomes dynamically unstable during their evolution. In less then a percent of triples the secondary or tertiary fills its Roche lobe before any other star does. One interesting sub-group is that were the secondary star starts transferring mass to a compact object. With a Galactic birthrate of 1-2 per 10000yrs, these sources can give rise to novae and x-ray emission without any prior phase of mass transfer or common-envelope evolution.

When we compare our evolving triple population with a population of pure binaries in the same mass range, we find that mass transfer takes place in a larger percentage of triples; 66-77% versus 28-39% respectively. This is in part because the presence of the tertiary star drives the inner binary to mass transfer, but mostly because the inner binaries of triples tend to be more compact compared to isolated binaries (Fig. 3). Another difference between triple and binary evolution is that in triples the orbits are not typically circularised upon mass transfer. About 40% of cases the orbit is still significantly eccentric (Figs. 8 and 10). Typically when the donor stars are fairly un-evolved upon Roche lobe overflow (e.g. on the main-sequence), the orbits are eccentric, and vice versa.

In this paper, we focus on triple evolution up onto the first phase of mass transfer, but if the triple system survives the interaction, more mass transfer phases can follow. We leave the outcome of the mass transfer phases to forthcoming papers. Assuming that mass transfer often leads to a stellar merger or dissolution of the triple only about 20-30% of triples survive for a Hubble time.

Our main conclusions are relatively robust to uncertainties in the primordial population of triples (in contrast with binary evolution). Eventhough we start with very different input distributions for the orbits in the triples, the resulting initial distributions

are more similar due to the removal of dynamical unstable systems. Such systems typically dissolve on dynamical timescales such that stellar evolution is less relevant.

We have also provided a simple tool (Fig. 4) with which one can estimate the dynamical impact of the tertiary star on the inner binary - for any given triple. An interactive version of Fig. 4a is available at https://bndr.it/wr64f. The graphical interface allows the user to adjust the figure to any given triple.

References

Abt, H. A. 1983, ARA&A, 21, 343
Antognini, J. M., Shappee, B. J., Thompson, T. A., & Amaro-Seoane, P. 2014, MNRAS, 439, 1079
Antognini, J. M. O. 2015, MNRAS, 452, 3610
Antonini, F., Murray, N., & Mikkola, S. 2014, ApJ, 781, 45
Antonini, F. & Perets, H. B. 2012, ApJ, 757, 27
Antonini, F., Toonen, S., & Hamers, A. S. 2017, ApJ, 841, 77
Bataille, M., Libert, A.-S., & Correia, A. C. M. 2018, MNRAS, 479, 4749
Belczynski, K., Kalogera, V., & Bulik, T. 2002, ApJ, 572, 407
Blaes, O., Lee, M. H., & Socrates, A. 2002, ApJ, 578, 775
Bobrick, A., Davies, M. B., & Church, R. P. 2017, MNRAS, 467, 3556
Bode, J. N. & Wegg, C. 2014, MNRAS, 438, 573
Boffin, H. M. J., Hillen, M., Berger, J. P., et al. 2014, A&A, 564, A1
Bonačić Marinović, A. A., Glebbeek, E., & Pols, O. R. 2008, A&A, 480, 797
Bondi, H. & Hoyle, F. 1944, MNRAS, 104, 273
Borkovits, T., Csizmadia, S., Paragi, Z., et al. 2010, in Astronomical Society of the Pacific Conference Series, Vol. 435, Binaries - Key to Comprehension of the Universe, ed. A. Prša & M. Zejda, 217
Borkovits, T., Forgács-Dajka, E., & Regály, Z. 2004, A&A, 426, 951
Chen, Z., Ivanova, N., & Carroll-Nellenback, J. 2019, arXiv e-prints, arXiv:1910.08027
Claeys, J. S. W., Pols, O. R., Izzard, R. G., Vink, J., & Verbunt, F. W. M. 2014, A&A, 563, A83
Comerford, T. A. F., Izzard, R. G., Booth, R. A., & Rosotti, G. 2019, MNRAS, 490, 5196
de Kool, M. & Ritter, H. 1993, A&A, 267, 397
de Vries, N., Portegies Zwart, S., & Figueira, J. 2014, MNRAS, 438, 1909
Dosopoulou, F. & Kalogera, V. 2016, ApJ, 825, 71
Duchêne, G. & Kraus, A. 2013, ARA&A, 51, 269
Duquennoy, A. & Mayor, M. 1991, A&A, 248, 485
Eggleton, P. P. 1983, ApJ, 268, 368
Eggleton, P. P. 2009, MNRAS, 399, 1471
Eggleton, P. P. & Tokovinin, A. A. 2008, MNRAS, 389, 869
Eldridge, J. J. 2009, MNRAS, 400, L20
Fabrycky, D. & Tremaine, S. 2007, ApJ, 669, 1298
Farihi, J., Becklin, E. E., & Zuckerman, B. 2005, ApJS, 161, 394
Ford, E. B., Kozinsky, B., & Rasio, F. A. 2000, ApJ, 535, 385
Frank, J., King, A., & Raine, D. J. 2002, Accretion Power in Astrophysics: Third Edition, 398
Gao, Y., Correia, A. C. M., Eggleton, P. P., & Han, Z. 2018, MNRAS, 479, 3604
Gualandris, A., Portegies Zwart, S., & Eggleton, P. P. 2004, MNRAS, 350, 615
Hamers, A. S. 2019, MNRAS, 482, 2262
Hamers, A. S. & Dosopoulou, F. 2019, ApJ, 872, 119
Hamers, A. S., Pols, O. R., Claeys, J. S. W., & Nelemans, G. 2013, MNRAS, 430, 2262
Hamers, A. S. & Thompson, T. A. 2019a, arXiv e-prints, arXiv:1907.08297
Hamers, A. S. & Thompson, T. A. 2019b, ApJ, 882, 24
Han, Z., Podsiadlowski, P., Maxted, P. F. L., Marsh, T. R., & Ivanova, N. 2002, MNRAS, 336, 449
Harrington, R. S. 1968, AJ, 73, 190
Heggie, D. C. 1975, MNRAS, 173, 729
Hollands, M. A., Tremblay, P.-E., Gänsicke, B. T., Gentile-Fusillo, N. P., & Toonen, S. 2018, MNRAS, 480, 3942
Huang, S. S. 1956, AJ, 61, 49
Huang, S.-S. 1963, ApJ, 138, 471
Hurley, J. R., Pols, O. R., & Tout, C. A. 2000, MNRAS, 315, 543
Hurley, J. R., Tout, C. A., & Pols, O. R. 2002, MNRAS, 329, 897
Hut, P. 1980, A&A, 92, 167
Hut, P. 1981, A&A, 99, 126

Iben, Jr., I. & Tutukov, A. V. 1999, ApJ, 511, 324
Innanen, K. A., Zheng, J. Q., Mikkola, S., & Valtonen, M. J. 1997, AJ, 113, 1915
Izzard, R. G., Glebbeek, E., Stancliffe, R. J., & Pols, O. R. 2009, A&A, 508, 1359
Kashi, A. & Soker, N. 2018, MNRAS, 480, 3195
Katz, B. & Dong, S. 2012, ArXiv e-prints
Katz, B., Dong, S., & Malhotra, R. 2011, Physical Review Letters, 107, 181101
Kervella, P., Thévenin, F., & Lovis, C. 2017, A&A, 598, L7
Kinoshita, H. & Nakai, H. 1999, Celestial Mechanics and Dynamical Astronomy, 75, 125
Kippenhahn, R. & Weigert, A. 1990, Stellar Structure and Evolution
Kiseleva, L. G., Eggleton, P. P., & Mikkola, S. 1998, MNRAS, 300, 292
Kiseleva, L. G., Eggleton, P. P., & Orlov, V. V. 1994, MNRAS, 270, 936
Kochanek, C. S. 1992, ApJ, 385, 604
Kouwenhoven, M. B. N., Brown, A. G. A., Portegies Zwart, S. F., & Kaper, L. 2007, A&A, 474, 77
Kozai, Y. 1962, AJ, 67, 591
Kroupa, P., Tout, C. A., & Gilmore, G. 1993, MNRAS, 262, 545
Lajoie, C.-P. & Sills, A. 2011, ApJ, 726, 67
Layton, J. T., Blondin, J. M., Owen, M. P., & Stevens, I. R. 1998, New A, 3, 111
Li, G., Naoz, S., Holman, M., & Loeb, A. 2014, ApJ, 791, 86
Lidov, M. L. 1962, Planet. Space Sci., 9, 719
Lithwick, Y. & Naoz, S. 2011, ApJ, 742, 94
Liu, B., Muñoz, D. J., & Lai, D. 2015, MNRAS, 447, 747
Lu, C. X. & Naoz, S. 2019, MNRAS, 484, 1506
Luo, L., Katz, B., & Dong, S. 2016, MNRAS, 458, 3060
Maeder, A. & Meynet, G. 2000, ARA&A, 38, 143
Malogolovets, E. V., Balega, Y. Y., & Rastegaev, D. A. 2007, Astrophysical Bulletin, 62, 111
Mardling, R. & Aarseth, S. 1999, in NATO Advanced Science Institutes (ASI) Series C, Vol. 522, NATO Advanced Science Institutes (ASI) Series C, ed. B. A. Steves & A. E. Roy, 385
Mardling, R. A. 1995, ApJ, 450, 732
Mardling, R. A. & Aarseth, S. J. 2001, MNRAS, 321, 398
Mazeh, T. & Shaham, J. 1979, A&A, 77, 145
McMillan, S. L. W. 1986, ApJ, 306, 552
Mennekens, N., Vanbeveren, D., De Greve, J. P., & De Donder, E. 2010, A&A, 515, A89
Michaely, E. & Perets, H. B. 2014, ApJ, 794, 122
Moe, M. & Di Stefano, R. 2017, ApJS, 230, 15
Moe, M. & Kratter, K. M. 2018, ApJ, 854, 44
Mohamed, S. & Podsiadlowski, P. 2007, Astronomical Society of the Pacific Conference Series, Vol. 372, Wind Roche-Lobe Overflow: a New Mass-Transfer Mode for Wide Binaries, ed. R. Napiwotzki & M. R. Burleigh, 397
Naoz, S. 2016, ARA&A, 54, 441
Naoz, S. & Fabrycky, D. C. 2014, ApJ, 793, 137
Naoz, S., Farr, W. M., Lithwick, Y., Rasio, F. A., & Teyssandier, J. 2013, MNRAS, 431, 2155
Nelemans, G., Yungelson, L. R., Portegies Zwart, S. F., & Verbunt, F. 2001, A&A, 365, 491
Nicholls, C. P. & Wood, P. R. 2012, MNRAS, 421, 2616
Perets, H. B. & Kratter, K. M. 2012, ApJ, 760, 99
Perpinyà-Vallès, M., Rebassa-Mansergas, A., Gänsicke, B. T., et al. 2019, MNRAS, 483, 901
Peters, P. C. 1964, Physical Review, 136, 1224
Petrova, A. V. & Orlov, V. V. 1999, AJ, 117, 587
Pijloo, J. T., Caputo, D. P., & Portegies Zwart, S. F. 2012, MNRAS, 424, 2914
Portegies Zwart, S. & Leigh, N. W. C. 2019, ApJ, 876, L33
Portegies Zwart, S. & McMillan, S. 2018, Astrophysical Recipes; The art of AMUSE
Portegies Zwart, S., McMillan, S., Harfst, S., et al. 2009, New A, 14, 369
Portegies Zwart, S., McMillan, S. L. W., van Elteren, E., Pelupessy, I., & de Vries, N. 2013, Computer Physics Communications, 183, 456
Portegies Zwart, S. F. & van den Heuvel, E. P. J. 2016, MNRAS, 456, 3401
Portegies Zwart, S. F. & Verbunt, F. 1996, A&A, 309, 179
Portegies Zwart, S. F. & Yungelson, L. R. 1998, A&A, 332, 173
Press, W. H. & Teukolsky, S. A. 1977, ApJ, 213, 183
Raghavan, D., McAlister, H. A., Henry, T. J., et al. 2010, ApJS, 190, 1
Raguzova, N. V. & Popov, S. B. 2005, Astronomical and Astrophysical Transactions, 24, 151
Regös, E., Bailey, V. C., & Mardling, R. 2005, MNRAS, 358, 544
Remage Evans, N. 2011, Bulletin de la Societe Royale des Sciences de Liege, 80, 663
Ruiter, A. J., Belczynski, K., & Fryer, C. 2009, ApJ, 699, 2026
Saladino, M. I., Pols, O. R., van der Helm, E., Pelupessy, I., & Portegies Zwart, S. 2018, A&A, 618, A50
Sana, H., de Mink, S. E., de Koter, A., et al. 2012, Science, 337, 444
Sana, H., Le Bouquin, J.-B., Lacour, S., et al. 2014, ApJS, 215, 15

Scholz, R.-D., Lodieu, N., Ibata, R., et al. 2004, MNRAS, 347, 685
Sepinsky, J. F., Willems, B., & Kalogera, V. 2007a, ApJ, 660, 1624
Sepinsky, J. F., Willems, B., Kalogera, V., & Rasio, F. A. 2007b, ApJ, 667, 1170
Sepinsky, J. F., Willems, B., Kalogera, V., & Rasio, F. A. 2009, ApJ, 702, 1387
Seto, N. 2013, Physical Review Letters, 111, 061106
Shappee, B. J. & Thompson, T. A. 2013, ApJ, 766, 64
Smeyers, P. & Willems, B. 2001, A&A, 373, 173
Soker, N. 2000, A&A, 357, 557
Teyssandier, J., Naoz, S., Lizarraga, I., & Rasio, F. A. 2013, ApJ, 779, 166
Tokovinin, A. 2008, MNRAS, 389, 925
Tokovinin, A. 2010, VizieR Online Data Catalog, 738
Tokovinin, A. 2014, AJ, 147, 87
Tokovinin, A. 2016, ApJ, 831, 151
Tokovinin, A. 2017, ApJ, 844, 103
Tokovinin, A. & Kiyaeva, O. 2016, MNRAS, 456, 2070
Tokovinin, A. & Latham, D. W. 2017, ApJ, 838, 54
Toonen, S., Claeys, J. S. W., Mennekens, N., & Ruiter, A. J. 2014, A&A, 562, A14
Toonen, S., Hamers, A., & Portegies Zwart, S. 2016, Computational Astrophysics and Cosmology, 3, 6
Toonen, S., Hollands, M., Gänsicke, B. T., & Boekholt, T. 2017, A&A, 602, A16
Toonen, S., Nelemans, G., & Portegies Zwart, S. 2012, A&A, 546, A70
Toonen, S., Perets, H. B., & Hamers, A. S. 2018a, A&A, 610, A22
Toonen, S., Perets, H. B., Igoshev, A. P., Michaely, E., & Zenati, Y. 2018b, A&A, 619, A53
van den Berk, J., Portegies Zwart, S. F., & McMillan, S. L. W. 2007, MNRAS, 379, 111
van der Helm, E., Portegies Zwart, S., & Pols, O. 2016, MNRAS, 455, 462
van Haaften, L. M., Nelemans, G., Voss, R., et al. 2013, A&A, 552, A69
Van Winckel, H., Waelkens, C., & Waters, L. B. F. M. 1995, A&A, 293
Vos, J., Østensen, R. H., Marchant, P., & Van Winckel, H. 2015, A&A, 579, A49
Walter, R., Lutovinov, A. A., Bozzo, E., & Tsygankov, S. S. 2015, A&A Rev., 23, 2
Wegner, G. & McMahan, R. K. 1988, AJ, 96, 1933
Xu, X.-B., Xia, F., & Fu, Y.-N. 2015, Research in Astronomy and Astrophysics, 15, 1857
Yungelson, L. R., Tutukov, A. V., & Livio, M. 1993, ApJ, 418, 794
Zavala, R. T., Hummel, C. A., Boboltz, D. A., et al. 2010, ApJ, 715, L44
Zavala, R. T., Hummel, C. A., Boboltz, D. A., et al. 2017, ApJ, 843, L18